CANADIAN THESES ON MICROFICHE

THÈSES CANADIENNES SUR MICROFICHE

National Library of Canada
Collections Development Branch

Canadian Theses on
Microfiche Service

Ottawa, Canada
K1A 0N4

Bibliothèque nationale du Canada
Direction du développement des collections

Service des thèses canadiennes
sur microfiche

NOTICE

The quality of this microfiche is heavily dependent upon the quality of the original thesis submitted for microfilming. Every effort has been made to ensure the highest quality of reproduction possible.

If pages are missing, contact the university which granted the degree.

Some pages may have indistinct print especially if the original pages were typed with a poor typewriter ribbon or if the university sent us an inferior photocopy.

Previously copyrighted materials (journal articles, published tests, etc.) are not filmed.

Reproduction in full or in part of this film is governed by the Canadian Copyright Act, R.S.C. 1970, c. C-30. Please read the authorization forms which accompany this thesis.

AVIS

La qualité de cette microfiche dépend grandement de la qualité de la thèse soumise au microfilmage. Nous avons tout fait pour assurer une qualité supérieure de reproduction.

S'il manque des pages, veuillez communiquer avec l'université qui a conféré le grade.

La qualité d'impression de certaines pages peut laisser à désirer, surtout si les pages originales ont été dactylographiées à l'aide d'un ruban usé ou si l'université nous a fait parvenir une photocopie de qualité inférieure.

Les documents qui font déjà l'objet d'un droit d'auteur (articles de revue, examens publiés, etc.) ne sont pas microfilmés.

La reproduction, même partielle, de ce microfilm est soumise à la Loi canadienne sur le droit d'auteur, SRC 1970, c. C-30. Veuillez prendre connaissance des formules d'autorisation qui accompagnent cette thèse.

THIS DISSERTATION
HAS BEEN MICROFILMED
EXACTLY AS RECEIVED

LA THÈSE A ÉTÉ
MICROFILMÉE TELLE QUE
NOUS L'AVONS REÇUE

Canada

NL 339 (r. 86/09)

Phase Behavior of the Naphthalene-Carbon Dioxide System at Supercritical Fluid Conditions

by

Poh Leng Cheong

A thesis
presented to the University of Ottawa
in fulfillment of the
thesis requirement for the degree of
Master of Applied Science
in
Chemical Engineering

Ottawa, Ontario, 1985

ABSTRACT

The high-pressure phase behavior of naphthalene(1)-carbon dioxide(2) system was experimentally investigated. The pressure-temperature-composition (P-T-x) section of the three-phase (solid-liquid-gas) coexistence curve was measured using a new technique. A correlation method of T-x relation of the three-phase curve was presented in this study. Solubility values of naphthalene in supercritical carbon dioxide were measured at 308.15 K and 332.15 K over a pressure range of 7.8 to 32.5 MPa using a flow system. These values were correlated by the Soave-Redlich-Kwong (SRK) equation of states with two random mixing rules.

A temperature minimum was found at 13.3 MPa and 331.73 K in the P-T projection. Liquid-gas equilibrium compositions were found between 12.7 MPa and 17.0 MPa for the 332.15 K isotherm. The liquid-phase compositions of naphthalene were found to be 0.484 and 0.320 at 12.7 MPa and 17.0 MPa respectively using the T-x correlation. It was found that the two-parameter random mixing rules were much better than the one-parameter random mixing rules in correlating the solubility values. However, the SRK equation of states and these mixing rules were unable to predict the complicated phase behavior of the 332.15 K isotherm.

ACKNOWLEDGMENTS

The author would like to acknowledge the guidance and advice of his research director, Dr. Benjamin C.-Y. Lu, Professor of Chemical Engineering, without whose encouragement and direction the completion of this work would not have been possible.

The author would also like to express his sincere thanks to Dr. K. Ohgaki, Assistant Professor of Chemical Engineering of the Osaka University, for his helpful discussions and invaluable suggestions. Thanks are also to Mr. J.-M. Yu for his help with the computation as well as Mr. J. Gasperetti, and his assistants, D. Lefebvre and A. Bonaldo, for their technical assistance and construction of the experimental apparatus.

Finally, the author is grateful to the University of Ottawa and the Ontario Ministry of Colleges and Universities for providing research scholarships.

TABLE OF CONTENTS

FIGURES

TABLES

NOMENCLATURE

A_{12}, A_{21}	Parameters in the van Laar equation
a,b,A,B	Variables in the SRK equation of state
f	Fugacity, MPa
ΔG_f	Gibbs free energy change of fusion, J/mole
ΔS_f	Entropy change of fusion, J/(mole)(K)
ΔH_f	Heat of fusion, J/mole
x	Liquid-phase mole fraction
y	Gas-phase or fluid-phase mole fraction
v	Molar volume, cm^3/mole
P	Total pressure, MPa
T	Temperature, K
Z	Compressibility factor
k_{12}	Binary parameter for attractive term
l_{12}	Binary parameter for van der Waals volume
R	Gas constant, J/(mole)(K)

Tm	Melting temperature of component 1, K
e.f.	Enhancement factor
n	Number of mole
γ	Liquid-phase activity coefficient
ϕ	Fugacity coefficient
ω	Accentric factor
μ	Chemical potential
ρ	Density, g/cm^3

SUPERSCRIPTS

s	Solid
ℓ	Liquid
g	Gas
o	Pure state
sat	Saturated

SUBSCRIPTS

1	Heavy component
2	Light component

c	Critical
r	Reduced
ij	Component identification; i=1,2, j=1,2
12	Binary mixture

Chapter I

INTRODUCTION

In recent years, the idea of using solvents in their critical or supercritical state has received much attention. This separation process, known as supercritical fluid extraction (SFE), is based on the fact that a gas can exhibit enhanced extractive power when it is compressed isothermally, at a temperature greater than its critical temperature, to a pressure greater than its critical pressure [1,2]. A number of solvents, such as carbon dioxide [3], ethane [3], ethylene [3] and xenon [4], can be used as supercritical solvents. Carbon dioxide is the most commonly used supercritical solvent. It not only has easily-reached critical conditions (T_c = 304.2 K, P_c = 7.38 MPa), but also is nontoxic, noncorrosive, nonflammable, readily-available and relatively inexpensive.

Supercritical fluid extraction has certain unique physico-chemical characteristics which distillation and liquid extraction do not have. In distillation, the separation factor (relative volatility) is primarily a function of temperature whereas liquid extraction is based on those properties of the material which determine the intermolecular interaction with the molecules of the extraction agent. Both of these effects are, to a certain extent, united in the supercritical fluid extraction. As shown in Table 1.1, while the density of a supercritical fluid is about 70% that of a normal liquid, the diffusivity and viscosity are intermedi-

ate to that of a liquid and a gas [5]. These characteristics are good enough to provide solvent capability and low enough for high diffusivity. Thus a supercritical fluid has better mass transfer characteristics than a liquid solvent. Figure 1.1 shows some P-ρ isotherms for pure carbon dioxide at subcritical and supercritical conditions. The region that is of interest for supercritical fluid extraction is at conditions bounded approximately by $0.9 < T_r < 1.2$ and $P_r > 1.0$.

Supercritical fluid extraction offers several advantages over distillation and liquid extraction:

1. The operation of supercritical fluid extraction is relatively simple. Only temperature and pressure are to be controlled during the operation.
2. This technology frequently offers energy savings over distillation and the advantage of yielding purer, less thermal damaged solutes than by more conventional methods.
3. The enhanced solubility effect of supercritical fluid extraction is reversible because it is very sensitive to changes in the density of the fluid (i.e. the changes in temperature and pressure).
4. Solubility of components in supercritical fluids can be increased by several hundred percent by the addition to the fluid phase of small quantities (one mole percent) of a volatile, often polar, material (entrainer) [6].

The major disadvantage of supercritical fluid extraction is that it is a capital-intensive process.

As mentioned above, the separation factor of supercritical fluid extraction is a strong function of both temperature and pressure.

Table 1.1: Physical properties of a gas, a liquid and a supercritical fluid.

Property	Gas	Liquid	Supercritical fluid *
density (g/cm^3)	10^{-3}	1.0	0.7
diffusivity (cm^2/s)	10^{-1}	10^{-5}	10^{-3}
viscosity (g/cm/s)	10^{-4}	10^{-3}	10^{-4}

* Carbon dioxide at T_r=1.00 and P_r=1.88.

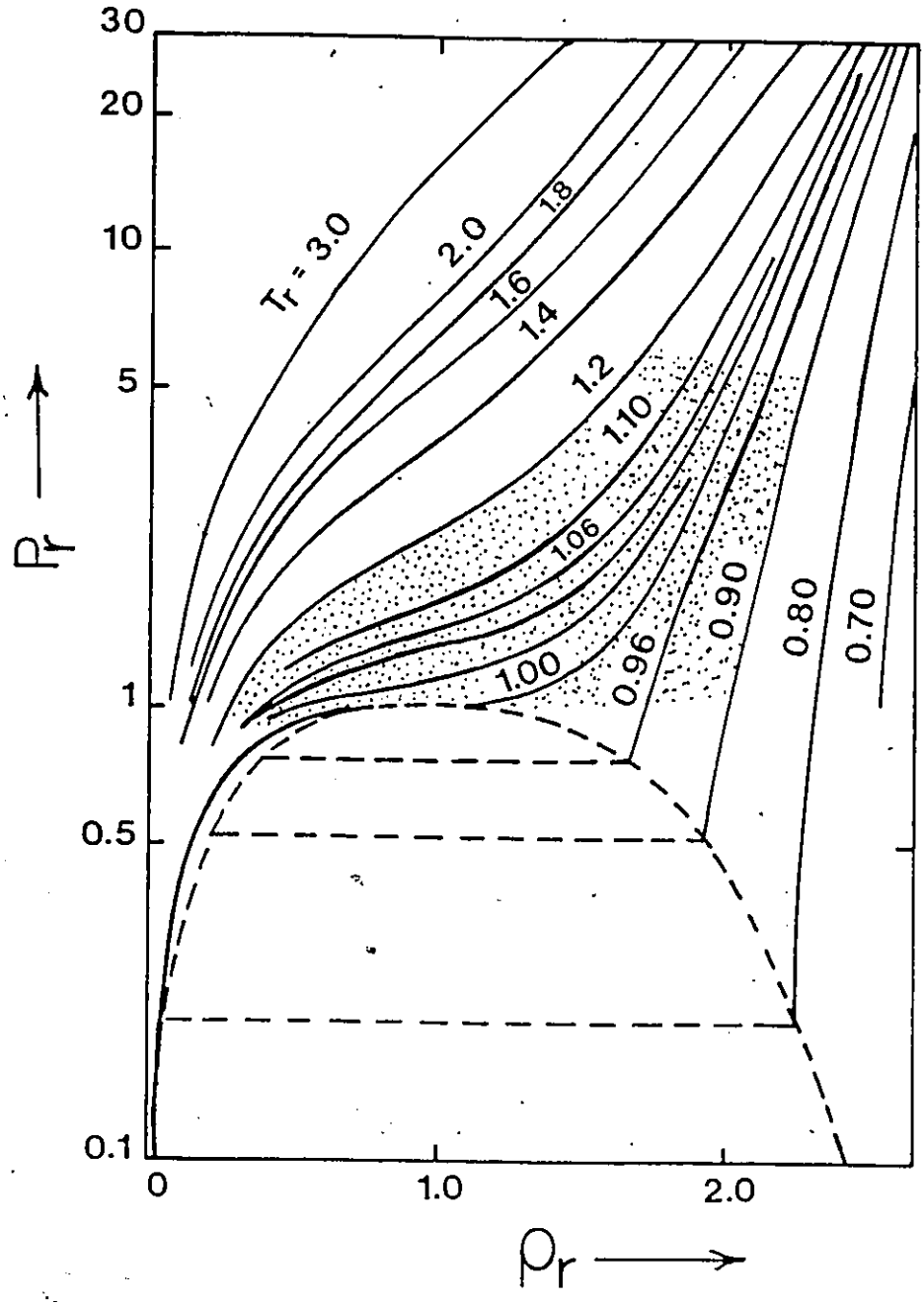

Figure 1.1: P-ρ phase diagram for carbon dioxide.

Novel separation schemes are possible by varying these two factors. For example, light components of coal can be extracted using supercritical fluid with a critical temperature below the temperature at which thermal degradation of the coal occurs [7]. The heavy solute can then be easily separated from the supercritical solvent by adjusting the density and hence solvent power of the supercritical fluids. If the pressure is lowered isothermally, the density decreases and the solute will precipitate from the solution. Alternatively, isobarically increasing the temperature near the critical pressure of the gas decreases the solvent density and hence precipitation of the solute can occur.

The most notable recent application of supercritical fluid extraction is the decaffeination of coffee by Hag AG in West Germany [8]. In the decaffeination process, presoaked green coffee beans are treated in a pressure vessel with carbon dioxide at 16-22 MPa (density $\sim$ 0.4-0.65 g/cm^3). The caffeine diffuses out of the beans into the supercritical carbon dioxide. The caffeine can be removed from the fluid phase by adjusting the density of supercritical carbon dioxide or alternatively by adsorbing the caffeine onto the activated carbon directly from the supercritical carbon dioxide.

Kerr-McGee Refining Corporation has already commercialized a process called Residuum Oil Supercritical Extraction (ROSE) that uses aliphatic hydrocarbons such as pentane at supercritical conditions as a solvent to extract asphaltenes and resins from distillation residues [9]. This technology has been extended to the de-ashing of coal liquids [10].

Chromatography using a supercritical fluid as a mobile phase to enhance migration of substances on chromatographic column was developed into a useful analytical technique [11]. Since a supercritical fluid has more desirable transport properties than a liquid, supercritical fluid chromatography (SFC) is superior to liquid chromatography in separation efficiency and speed. Pressure drop across the column in supercritical fluid chromatography is small since the supercritical fluid has a low viscosity. Supercritical fluid chromatography is also particularly useful for the separation of thermally labile, nonvolatile components such as porphyrins which decompose during temperature programmed gas chromatography.

Supercritical fluid extraction is also looking attractive for other applications in the chemical, food, drug and energy industries. These applications include extraction of organic pollutants from wastewater [12], extraction of citrus oil from peelings [12], extraction of pyrethrin insecticides from pyrethrum [12] and enhanced oil recovery by carbon dioxide injection [13].

Although a number of new applications is commercially viable at this moment, supercritical fluid technology has yet to live up to its early promise as an extraction method [12]. The main reason is that too little is known about the thermodynamics of supercritical systems. There is still a need for fundamental research with supercritical solvents, such as high-pressure phase equilibria of fluid mixtures, to fully understand and capitalize on the unique processing capabilities of these solvents. Supercritical fluid extraction involving the separation of relatively nonvolatile components, often in solid phase, has been investi-

gated lately by many researchers [1-5,14-20]. Most of them concentrated on the measurements of solubility data. In addition to the solubility measurements, McHugh et al. [3-5,14] also measured the pressure-temperature (P-T) projection of the three-phase (solid-liquid-gas) coexistence curve of binary mixtures. In their study, a large temperature minimum in the P-T projection was observed in the biphenyl-carbon dioxide, naphthalene-carbon dioxide and octacosane-carbon dioxide systems. Such unusual behavior was not observed in the ethane or ethylene systems. Because of the temperature minimum, some reported solubility data only describe a liquid-gas equilibrium. Therefore thermodynamic correlations based on solid-fluid assumption are no longer valid in certain pressure ranges near the upper critical end point (UCEP) temperature [3-5].

The objective of this research is to study the unusual phase behavior of naphthalene(1)-carbon dioxide(2) system. This system is chosen in this study because physical properties of both components are well-defined in the literature. A new technique was used to determine the three-dimensional pressure-temperature-composition (P-T-x) space model of the three-phase (S-L-G) coexistence curve. Both the lower critical end point (LCEP) and upper critical end point (UCEP) are of technological interest in supercritical fluid extraction. In the UCEP case, mole fractions are larger and phase behavior near the UCEP is interesting and of greater practical importance [3-5]. Thus solubility data near the UCEP temperature were experimentally investigated. Solubility data were measured by a flow system in this study [14-18].

In his recent phase theoretical investigations of carbon dioxide systems, Schneider [21-23] has shown that different classes of phase behavior can be characterized according to the shape of their critical curves. Two basic classes of P-T projection of phase behavior for binary mixtures of heavy hydrocarbons and carbon dioxide are classified and described briefly in chapter II.

A correlation method of T-x relation of the three-phase (S-L-G) coexistence curve is presented in this study. The van Laar equation was used to predict the liquid-phase activity coefficient of the heavy component. To correlate the solubility data, an empirical equation of state such as the Soave-Redlich-Kwong (SRK) was used. In addition to one-parameter random mixing rules (one-fluid model), two-parameter random mixing rules (binary parameters for both attractive term and van der Waals volume, a and b) were also used.

Chapter II

PHASE BEHAVIOR FOR BINARY MIXTURES OF CARBON DIOXIDE AND HEAVY HYDROCARBONS

The understanding of phase equilibria at high pressure is undoubtedly invaluable for the applications of supercritical fluids in chemical engineering processes. This involves the study of the phase relationships of mixtures at high pressure, which can best be expressed by P-T-x-y surfaces represented in graphical form or often by P-T, T-x-y or P-x-y projections of these surfaces on the appropriate plane.

Since supercritical fluid extraction usually involves the extraction of relatively nonvolatile components by a light supercritical fluid, the molecular size, shape, structure and critical conditions of the two components differ substantially. In some instances, the melting temperature of the heavy component 1, Tm, is much larger than the critical temperature of the light component 2, T_{C2}, and there is no common range of temperature in which both pure components are liquid. In this chapter, systems of this kind were classified according to the P-T projection of their phase diagrams. P-x-y sections of the mixtures at constant temperature were then deduced from the P-T projection and the phase behavior of the mixtures at high pressure is described using these isotherms.

2.1 Classification of Phase Behavior.

Because of the great variety of phase behavior of the mixtures, a comprehensive discussion of the phase behavior is inhibited unless different types of diagram are classified in some way. In the classification of phase diagrams of carbon dioxide systems, the most recent work is that of Chai [24] who classified the phase diagrams into four different categories. For the purpose of discussion, the phase behavior of carbon dioxide systems is classified in a simple way. Using as a basis the P-T projections of critical and three-phase lines, the phase behavior of the binary systems of interest is classified into two basic classes, as shown in Figure 2.1 and Figure 2.2.

In the diagrams, principal lines and points form the boundaries in the P-T space. The types of boundary lines are described as follows:

1. Pure component vapour pressure curves (M-C1 and F-C2), sublimation curve (M-E) and melting curve (M-D) are in solid lines.
2. Critical lines (O-C2, N-C1, LCEP-C2 and UCEP-C1) are in dashed lines.
3. Three-phase lines (B-Q, O-Q, M-Q, B-LCEP, M-UCEP and H-Q) are in dash-dot lines.

The types of points are described in a similar manner:

1. Triple point (M) of pure component 1 is in triangle.
2. Pure component critical points (C1 and C2) are in open circles.
3. Critical end points (O, LCEP and UCEP), formed by the intersection of a critical line with a three-phase lines liquid-liquid-gas or solid-liquid-gas, are in closed circles.

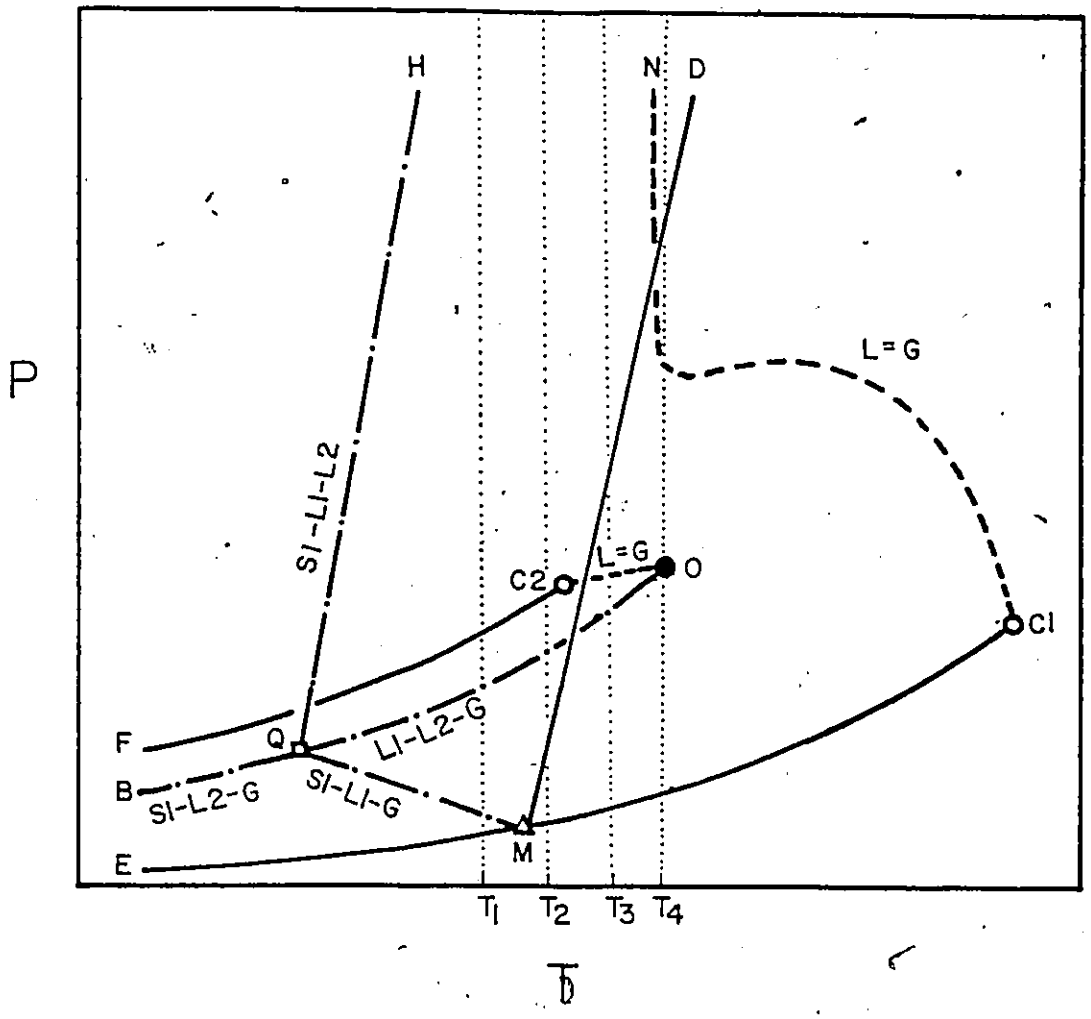

Figure 2.1: Schematic P-T projection of class I systems.

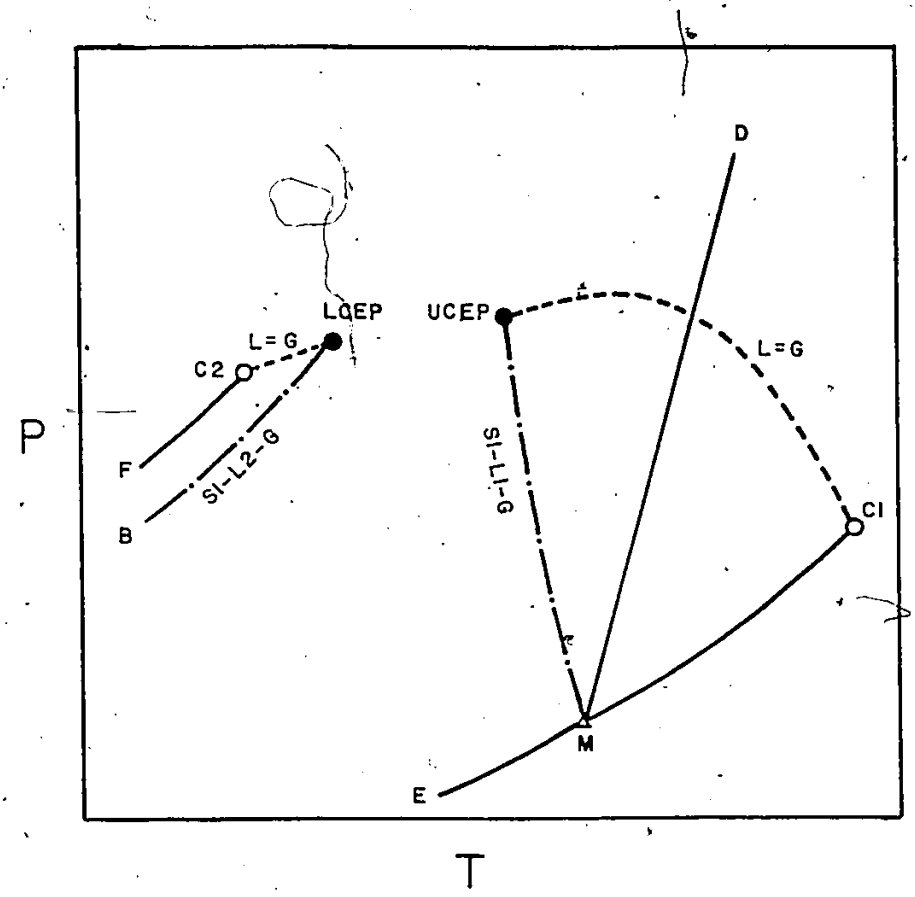

Figure 2.2: Schematic P-T projection of class II systems.

4. Quadruple point (Q) where four phases (S1-S2-L-G) in equilibruim is in open square.

2.2 Class I Systems.

Class I systems occur when the three-phase line S1-L1-G cuts a three-phase line of liquid-liquid-gas (L1-L2-G) at a quadruple point (S1-L1-L2-G), where L1 represents the component 1-rich phase and L2 represents the component 2-rich phase (Figure 2.1). The liquid-gas (L-G) critical line is not continuous from C1 to C2, but consists of two branches. One branch emerges from C2 and ends in the critical end point O, where it intersects the three-phase region (L1-L2-G). The second branch, emerging from C1, passes through maximum and minimum pressures, and then rises to very high pressure. Examples of this class include the trans-decalin-carbon dioxide [25], tetralin-carbon dioxide [26], 2-methylnaphthalene-carbon dioxide [27] and n-eicosane-carbon dioxide systems [28].

Figure 2.3 shows four P-x-y sections corresponding to T_1, T_2, T_3 and T_4 of Figure 2.1. For the isotherm at T_1 in Figure 2.3(a), there are two three-phase lines (S1-L1-G and L1-L2-G) at pressures below the saturated pressure of component 2 since these three-phase lines (M-Q and O-Q) are below the vapour pressure curve (F-C2) of component 2 at T_1 (Figure 2.1). The two-phase region at pressures below the three-phase line S1-L1-G (the first horizontal line) corresponds to solid-gas equilibrium whereas the two-phase region at pressures below the three-phase line L1-L2-G (the second horizontal line) corresponds to liquid-gas, solid-liquid or a single liquid phase (L1) depending on

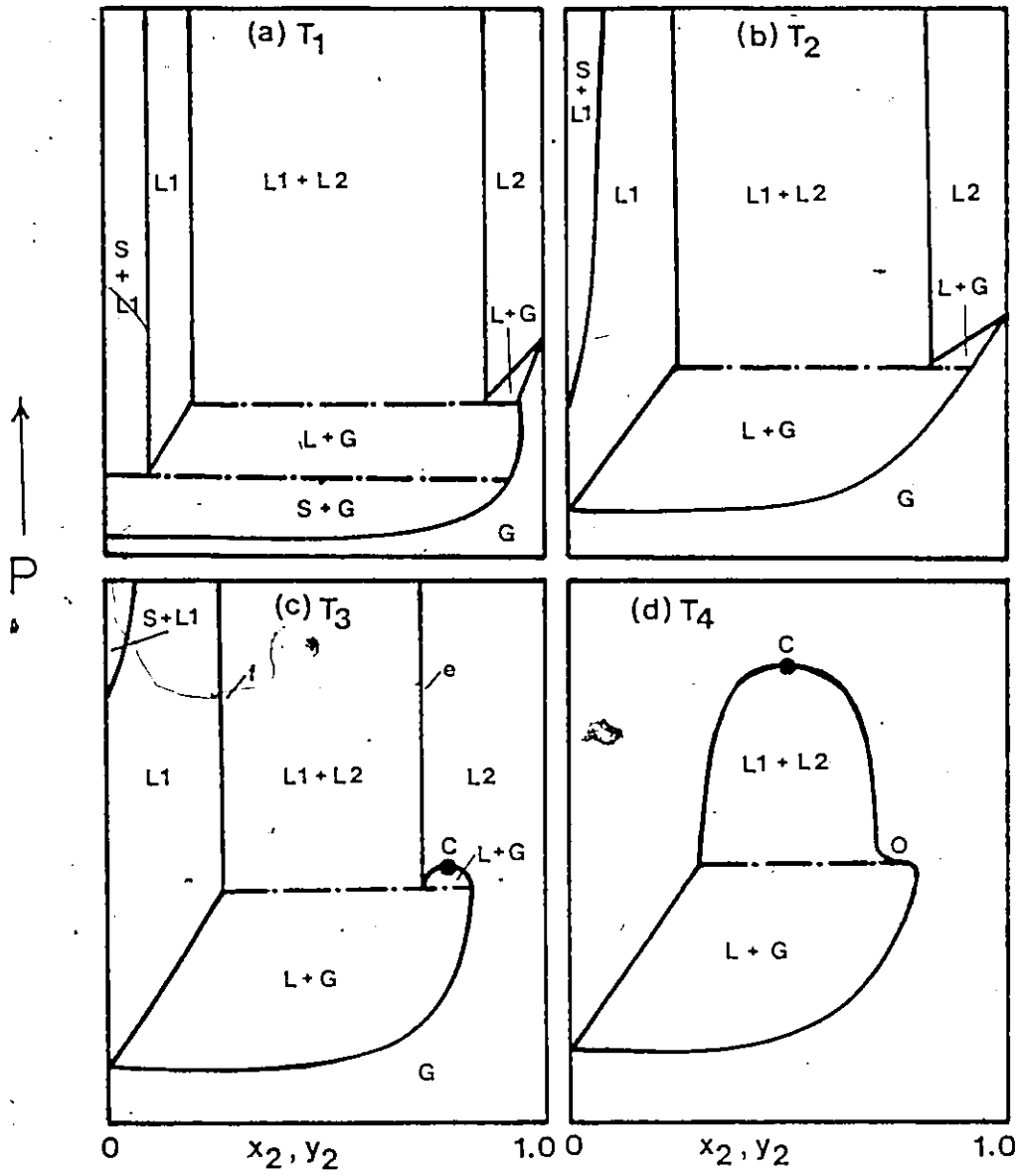

Figure 2.3: P-x-y isotherms of class I systems.

(a) $T_1 < Tm$, (b) $Tm < T_2 < T_{C2}$,

(c) $T_{C2} < T_3 < T_0$, (d) $T_4 = T_0$.

the mixture composition. At pressures above the three-phase line L1-L2-G, there is a small two-phase liquid-gas region occurs at high contents of component 2; additionally a liquid-liquid miscibility gap L1-L2 is found. Such miscibility gap is due to the very different volatilities of the pure components.

The isotherm (T_2) shown in Figure 2.3(b) is situated at a temperature between the melting temperature of component 1 (Tm) and the critical temperature of component 2 (T_{C2}). The three-phase line S1-L1-G disappears and the solid-liquid equilibrium appears at a higher pressure.

The isotherm (T_3) in Figure 2.3(c) cuts the liquid-gas critical locus (O-C2) at point C where the two-phase liquid-gas region vanishes at this point. Liquid-liquid miscibility gap still exists; but with a narrower gap, at pressures above the three-phase line. Here the branch "e" on the right represents the solubility of the liquid component 1 (heavy component) in the supercritical component 2 and the branch "f" on the left that of the supercritical component 2 in the liquid component 1.

The isotherm corresponding to T_4 shows that the small liquid-gas region decreases to zero at the critical end point O and the liquid-liquid miscibility gap closes at the liquid-liquid critical point. This is because the three-phase line L1-L2-G cuts the critical locus (O-C2) which emerges from the critical point of component 2 (C2). Beyond temperature T_4, the liquid-liquid and liquid-gas equilibrium can no longer be distinguished.

2.3 Class II Systems.

A binary mixture consisting of a nonvolatile solute and a near-critical or supercritical solvent of class II system is the system in which not only the critical temperatures of the pure components are far apart; but also the critical temperature of the solvent lies below the melting temperature (Tm) of the solute (Figure 2.2). In this case, the three-phase lines are of the type solid-liquid-gas (S-L-G), instead of the type liquid-liquid-gas (L-L-G) shown in the phase diagrams of the class I systems.

Class II systems occur as a result of the sequence of changes shown in Figure 2.4 [5,29]. Figure 2.4(a) is a typical P-T diagram for a binary mixture in which the components do not differ appreciably. As the molecular size, shape, structure and critical conditions of the two components differ substantially, i.e. the critical temperature of component 2 lies far below that of the melting temperature of component 1 , the three-phase region S1-L-G (line BM in Figure 2.4(a)) moves upward, and intersects the gas-liquid critical line (C1-C2) to form two critical end points, as shown in Figure 2.4(b). Such points are called, respectively, lower and upper critical end points (LCEP and UCEP), since they mark the limits of pressure and temperature in which critical states may be found. With increasing difference between the critical temperatures of the pure components, solid-liquid-gas (S1-L1-G) lines can be classified into three types [30], as shown in Figure 2.5.

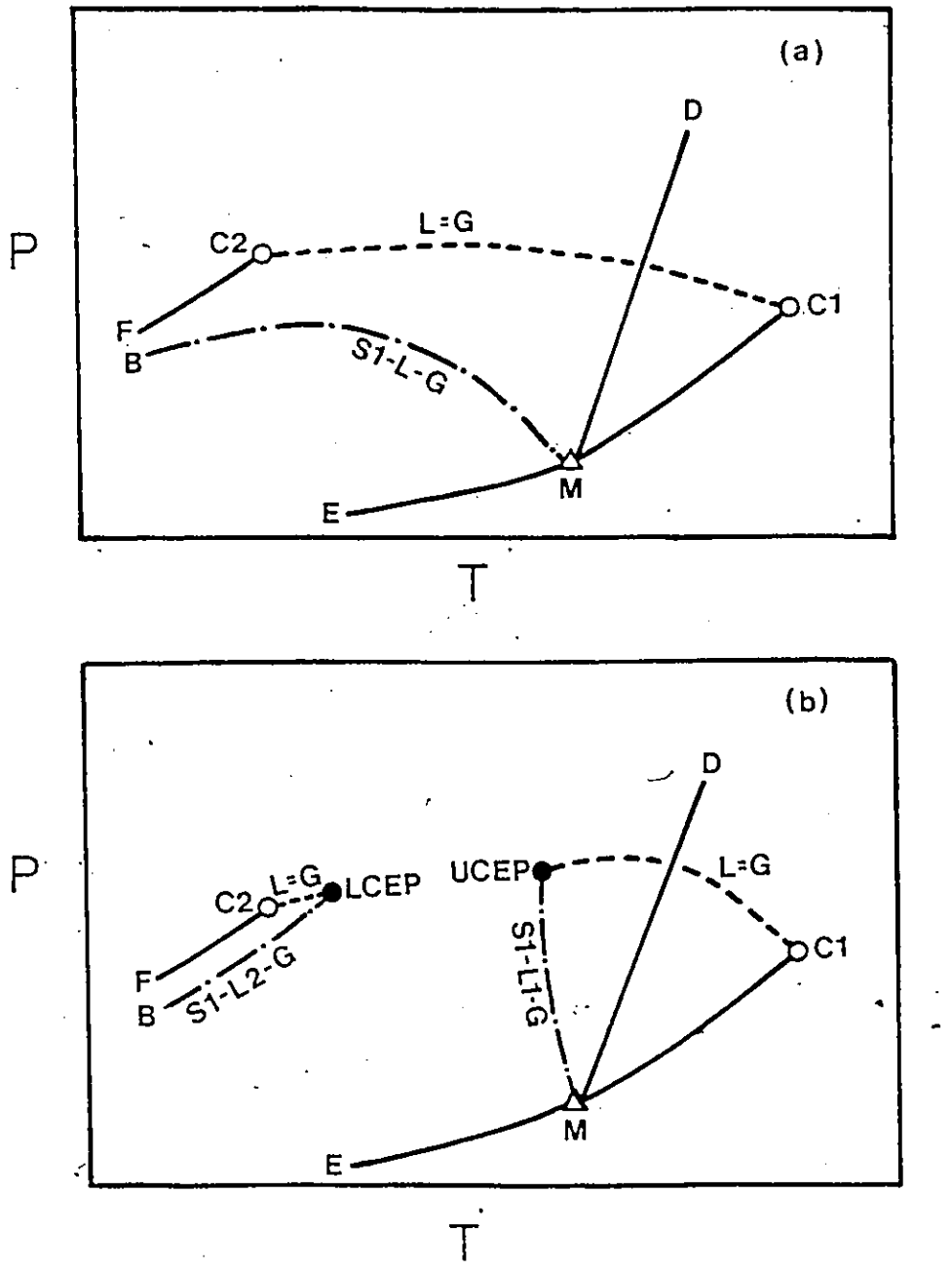

Figure 2.4: Formation of class II systems.

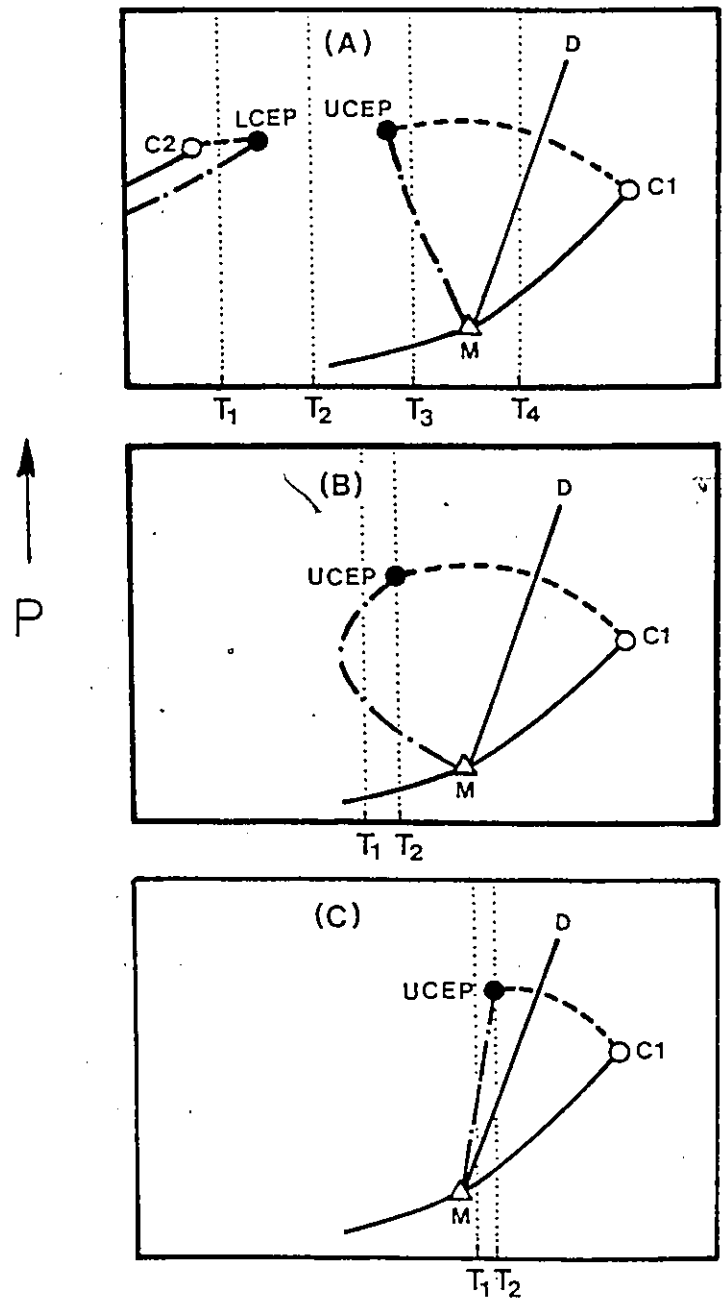

Figure 2.5: Three types of class II systems.

2.3.1 Class II(A) Systems.

The first type of class II systems (Figure 2.5(A)) is the most common type of system encountered in supercritical fluid extraction. The three-phase (S1-L1-G) line M-UCEP has a negative slope. Example includes diphenylamine-carbon dioxide (for reference see [29]). The three-sided region, M-UCEP-C1, bounded by the vapour pressure curve M-C1, the liquid-gas critical line C1-UCEP, and the three-phase line M-UCEP, is a region of liquid-gas phase separation. At temperatures between the UCEP and LCEP, the solid phase of component 1 is in equilibrium with a component 2-rich gas phase. No liquid phase exists in the temperature range between LCEP and UCEP.

Four P-x-y isotherms corresponding to the temperatures T_1, T_2, T_3 and T_4 of Figure 2.5(A) are shown in Figure 2.6. T_1 lies between T_{C2} and LCEP and it cuts both the three-phase line B-LCEP and the critical line C2-LCEP (see Figure 2.5(A)). In Figure 2.6(a), solid-gas equilibrium exists as the light component is compressed until the solid-liquid-gas line is reached. The three equilibrium phases are connected by a horizontal tie line and point C is the liquid-gas critical point. Since almost no gas dissolves in the solid phase, pure solid is assumed in this case. The asymmetric shape of the small liquid-gas region indicates that the solubility of the light component 2 in the heavy phase (left branch of the L-G region) increases much faster than the solubility of the heavy component in the light phase (right branch of the L-G region). Above the three-phase line, solid-fluid equilibrium is found.

As the temperature increases from T_1 to T_2, the liquid-gas region on the right of Figure 2.6(a) decreases in size, and vanishes at the

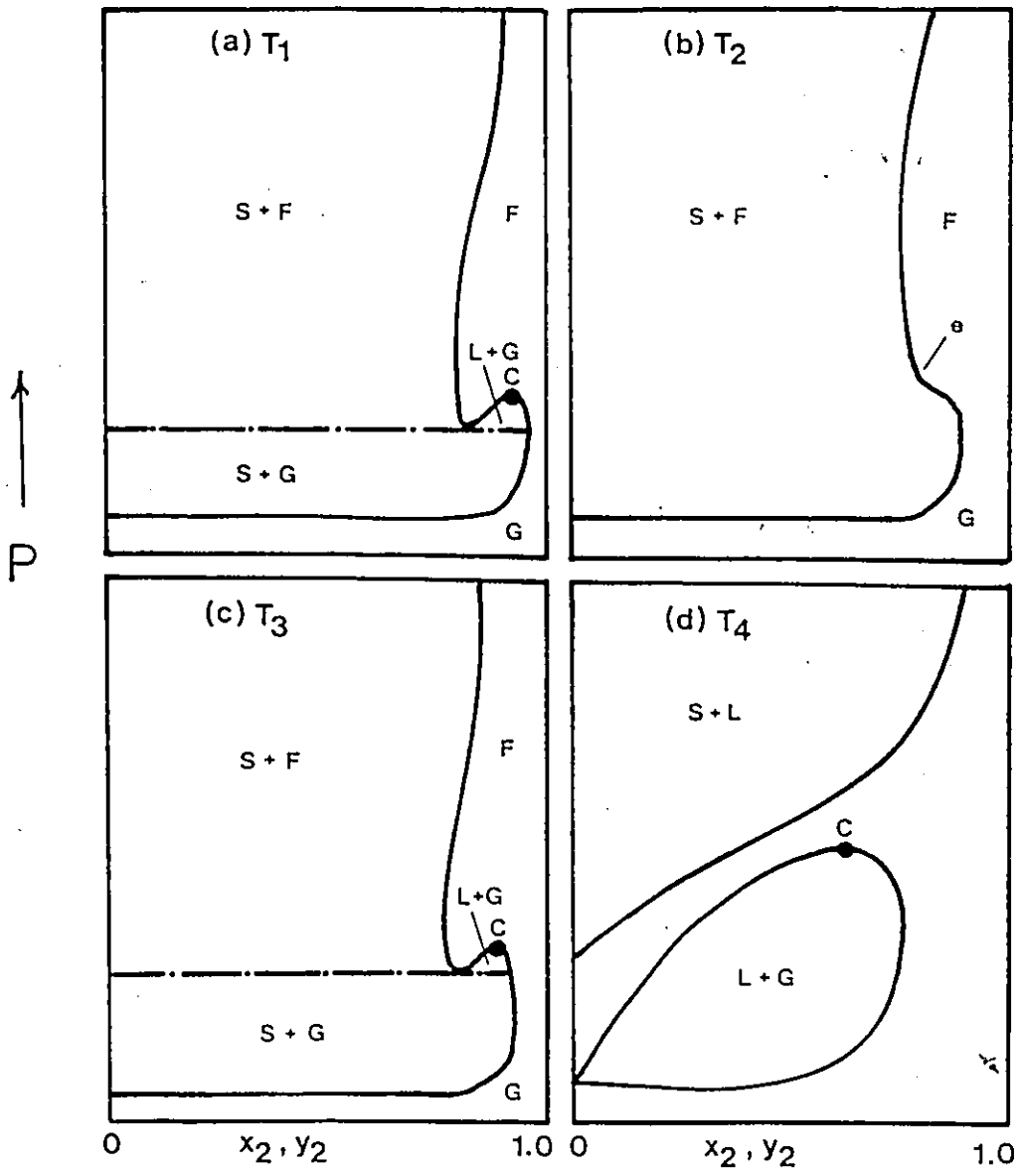

Figure 2.6: P-x-y isotherms of class II(A) systems.

(a) $T_{C2} < T_1 < T_{LCEP}$,

(b) $T_{LCEP} < T_2 < T_{UCEP}$,

(c) $T_{UCEP} < T_3 < Tm$, (d) $T_4 > Tm$.

LCEP. An isotherm at T_2 can be expected to have the shape shown in Figure 2.6(b). The branch "e" illustrates the behavior of enhanced solubility of a nonvolatile solute 1 in a supercritical solvent 2. With increasing pressure there is a dramatic increase in the solubility of component 1 in the supercritical fluid phase. Such solubility behavior is shown by the negative slope of the fluid boundary in this region (see branch "e"). Both experimental and theoretical studies suggest that there is a maximum solubility in the solid-fluid equilibrium [31-33].

The P-x-y isotherm depicted in Figure 2.6(c) is at a temperature less than the melting temperature of component 1 but slightly greater than the UCEP temperature. In this instance, the solubility behavior is similar to that in Figure 2.6(a). As the temperature increases from T_3 to T_4, farther from T_{UCEP}, the liquid-gas region increases in size. After passing the melting temperature of component 1, the solid-gas equilibrium vanishes and hence two completely separated two-phase regions, solid-liquid and liquid-gas phases, form as shown in Figure 2.6(d).

2.3.2 Class II(B) Systems.

In the second type of class II systems, the three-phase line M-UCEP has a temperature minimum and regions of both negative and positive slope (Figure 2.5(B)). Examples of this type include the naphthalene-carbon dioxide [3,5], biphenyl-carbon dioxide [3,5] and octacosane-carbon dioxide systems [3,5]. P-x-y isotherms below the temperature minimum (T_{min}) of the three-phase line are of little interest in this case since they are the same as Figure 2.6(a) and Figure 2.6(b).

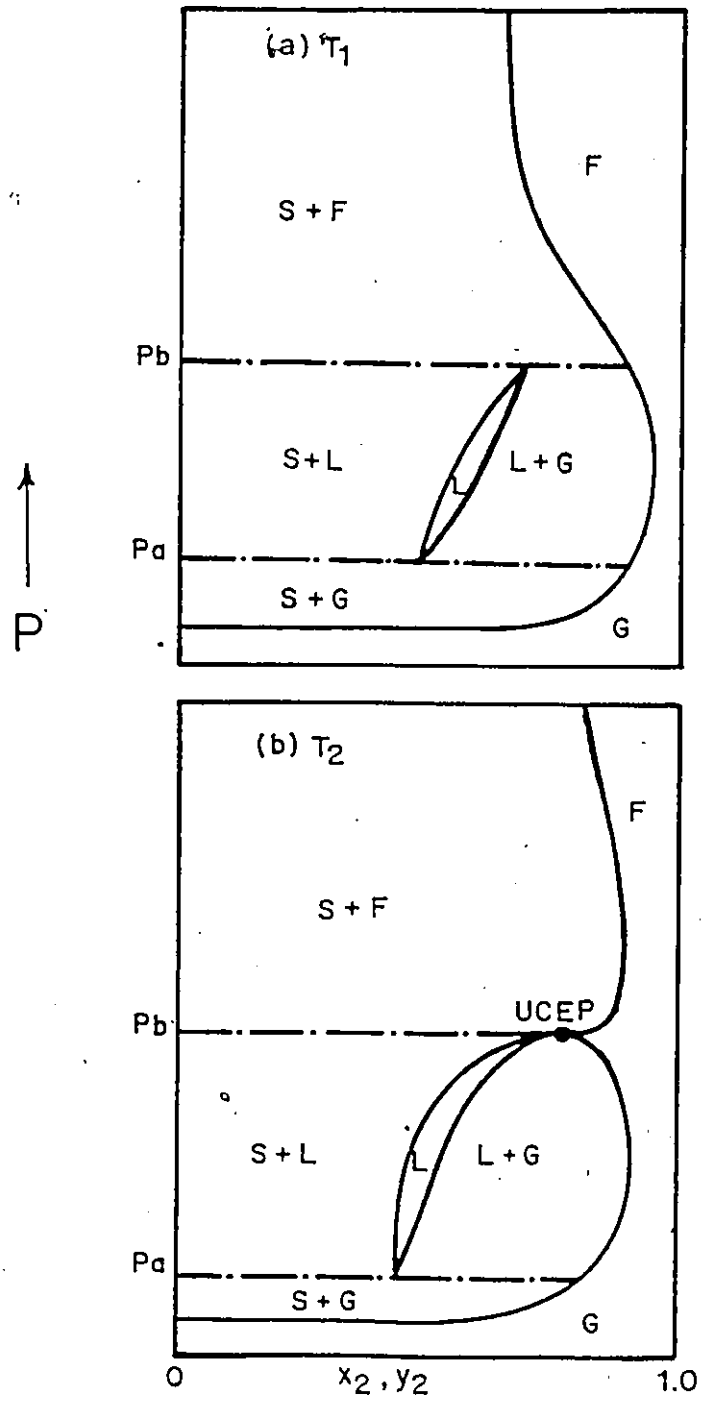

Figure 2.7: P-x-y isotherms of class II(B) systems.

(a) $T_{min} < T_1 < T_{UCEP}$, (b) $T_2 = T_{UCEP}$.

An isotherm at T_1, a temperature which is greater than the temperature minimum of the three-phase line (S1-L1-G) but still less than the UCEP temperature (see Figure 2.5(B)), is shown in Figure 2.7(a). A more complex phase behavior is expected since the three-phase line M-UCEP of Figure 2.5(B) is intersected twice at T_1. At pressures below the first three-phase pressure, Pa in Figure 2.7(a), solid-gas equilibrium exists. At pressures above the second three-phase pressure, Pb, solid-fluid equilibrium exists. Between Pa and Pb, either liquid-gas, solid-liquid or a single liquid phase exists depending on the composition of the mixture. Using a flow system, only the composition of the heavy component in the gas or fluid phase is sampled and analysed. The measured P-x-y isotherm represents the solid line on the right of Figure 2.7. Thus thermodynamic correlations of the solubility data using solid-fluid equilibrium are not valid between Pa and Pb. It is interesting to notice that the solid-liquid line bends toward compositions richer in the light component with increasing pressure and it eventually merges with the liquid branch of the liquid-gas loop. Mole fractions of both loops are considerably high.

For the isotherm at the UCEP temperature, shown in Figure 2.7(b), the three-phase line (S1-L1-G) intersects precisely at the UCEP pressure and the liquid-gas mixture becomes critical in the presence of excess solid. The derivative $(\partial P/\partial x)_{T_{UCEP}}$ must equal to zero at this point [34]. At pressure greater than the UCEP pressure, solid-fluid equilibrium is maintained again.

2.3.3 Class II(C) Systems.

In Figure 2.5(C), the critical and three-phase lines intersect at a critcal end point UCEP which lies at a temperature above the triple point (M) of component 1. The isotherm which lies below the triple point of component 1 is similar to that of the system described in Figure 2.6(b), which consists of a single region of solid-fluid equilibrium. At temperature (T_1) between the triple point of component 1 and the UCEP temperature, P-x-y isotherm is different from the systems shown previously (see Figure 2.8(a)). At pressures below the saturated vapour pressure of component 1, Pa, either liquid-gas or a single liquid phase exists depending on the composition of the mixture. However, between Pa and the three-phase pressure Pb, a solid-liquid region appears in addition to the two regions described above. Above Pb, solid-fluid equilibrium exists.

As the temperature increases to the UCEP temperature, the single liquid region (L) increases in size and the liquid-gas mixture becomes critical. At this point, the solid-liquid and solid-fluid regions become identical. Such an isotherm cannot be observed in class II(A) systems (Figure 2.6(d)) since the liquid-gas region cannot intersect with the solid-fluid region.

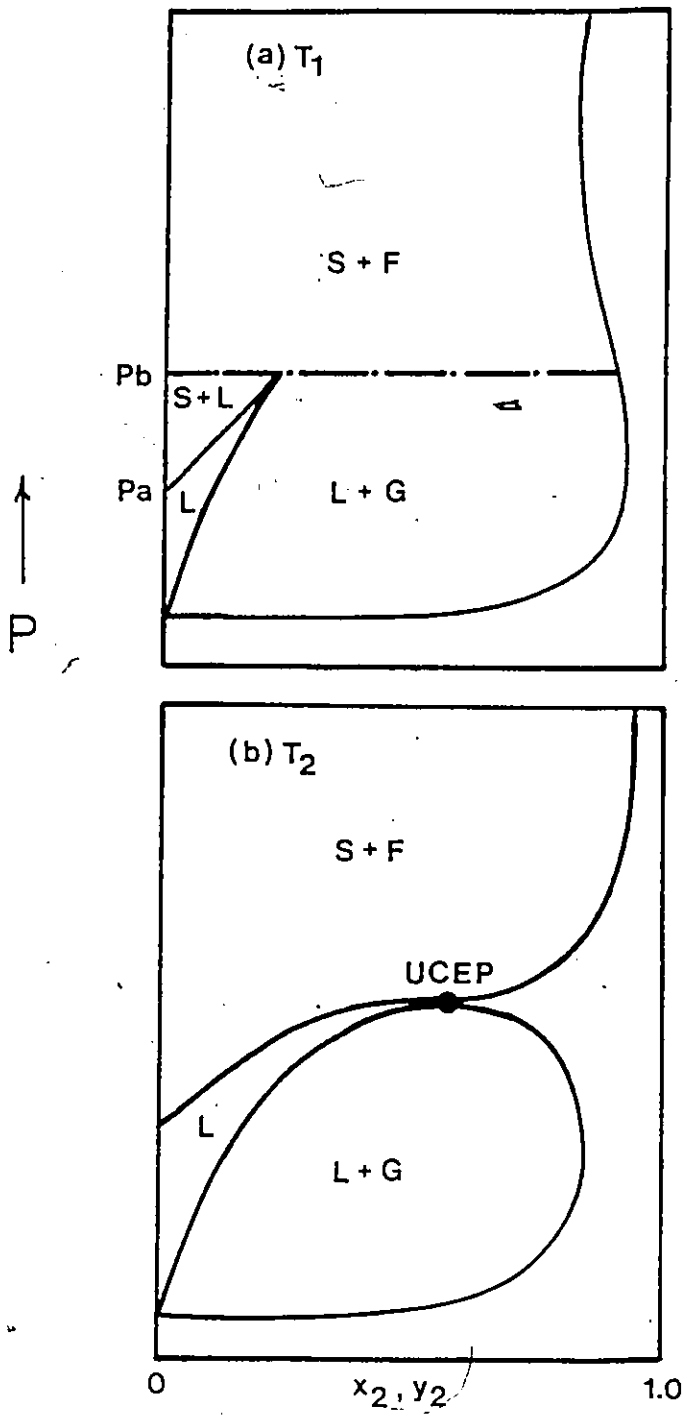

Figure 2.8: P-x-y isotherms of class II(C) systems.
(a) $Tm < T_1 < T_{UCEP}$, (b) $T_2 = T_{UCEP}$.

2.4 Representation of Phase Behavior.

Theoretical calculations are useful in correlating the experimental data and extending the experimental data to regions or systems not experimentally measured. In the following two sections, correlation methods for the T-x relation of the three-phase (S-L-G) lines and the solubility data using equation of state are presented.

2.4.1 Correlation of T-x Relation.

To correlate the T-x relation, solid-liquid equilibrium is assumed and the following expression is obtained:

$$\ln x_1\gamma_1 = -(\Delta H_f^0/R)(1/T-1/Tm) \qquad (2\text{-}1)$$

where x_1 and γ_1 are, respectively, the mole fraction and the activity coefficient of component 1 (heavy component) in liquid phase. ΔH_f^0 and Tm are the heat of fusion and the melting temperature of pure component 1 respectively while T is the system temperature. Rigorous derivation of eq.(2-1) is shown in Appendix A. In the derivation, correction terms containing ΔCp (the specific heat difference between liquid and solid phase) are neglected and ΔG_f^0 is assumed to be independent of pressure, i.e. the partial molar volume of liquid naphthalene is equal to that of solid naphthalene. The first assumption is made because both ΔCp of naphthalene and the temperature range of this study are small. The second assumption is made because of the lack of information of the partial molar volume of liquid and solid naphthalene.

Since the values of ΔH_f^0 and Tm are available in the literature, the T-x relation of the three-phase (S-L-G) line can be found if the activi-

ty coefficient γ_1 can be estimated. In this study, the van Laar equation is used to estimate the γ_1 because of its flexibility and its mathematic simplicity. The van Laar equation is illustrated in the following expression:

$$\ln\gamma_1 = A_{12}/\{1+(A_{12}/A_{21})(x_1/x_2)\}^2 \qquad (2\text{-}2)$$

Constants A_{12} and A_{21} are assumed to be temperature independent. This assumption is quite tolerable since the temperature range involved in this study is not large. Experimental data of γ_1, calculated from eq.(2-1), are used to find the best fitted values of A_{12} and A_{21} by minimizing the sum of squares of the difference between the calculated and experimental γ_1 values. Projection of T-x relation of the ideal solution is also included for comparison by letting γ_1 equal to unity.

2.4.2 Correlation of Solubility Data.

The thermodynamics applicable to relate the equilibrium mole fraction of a solid dissolved in a supercritical fluid was treated by Prausnitz [35] and the rigorous derivation is shown in Appendix B. The thermodynamic model can be expressed as follows:

$$y_1 = (P_1^{sat}/P)(1/\phi_1)\exp\{(v_1^s/RT)(P-P_1^{sat})\} \qquad (2\text{-}3)$$

$$\text{or} \quad y_1 = (P_1^{sat}/P)(e.f.) \qquad (2\text{-}4)$$

In eq.(2-3), several assumptions are made: (a) the solid is pure, (b) the solid is considered to be incompressible, and (c) the fugacity coef-

ficient of pure vapour 1 at T and P_1^{sat} is unity. In most instances, these assumptions are appropriate. In eq.(2-4), the Poynting factor (exponential term) seldoms gives an enhancement factor (e.f.) of more than 2 [35]. Thus the fugacity coefficient ϕ_1 accounts for the high enhancement factor encountered experimentally. Accurate estimates of this variable are therefore necessary to determine y_1. ϕ_1 can be estimated from an equation of state with mixing rules. In this study, the Soave [36] modification of the Redlich-Kwong equation of state [37] was used:

$$P = RT/(v-b) - a/\{v(v+b)\} \qquad (2\text{-}5)$$

To relate the pure component terms, one-parameter and two-parameter random mixing rules were used. The two-parameter random mixing rules were used in this study to account for the highly asymmetric nature of the mixtures. Using the one-parameter random mixing rules,

$$a = \Sigma\Sigma y_i y_j a_i^{0.5} a_j^{0.5} (1-k_{ij})$$
$$b = \Sigma y_i b_i \qquad (2\text{-}6)$$

the expression for ϕ_1 is illustrated as follows:

$$\ln\phi_1 = -\ln(Z-B) + (b_1/b)(Z-1)$$
$$- (A/B)\{2(a_1^{0.5}/a^{0.5})(b_1/b)\}\ln\{1+(B/Z)\} \qquad (2\text{-}7)$$

where $A = (aP)/(RT)^2$ and $B = (bP)/(RT)$

The two-parameter random mixing rules involve binary parameters for both the a and b terms:

$$a = \Sigma\Sigma y_i y_j a_i^{0.5} a_j^{0.5} (1-k_{ij})$$
$$b = \Sigma\Sigma y_i y_j \{(b_i+b_j)/2\}(1-l_{ij}) \qquad (2\text{-}8)$$

This yields the following expression for ϕ_1:

$$\ln\phi_1 = -\ln(Z-B) + (b_1'/b)/(v-b)$$
$$+ a\{1+(b_1'/b)\}/\{RT(v+b)\}$$
$$- (A/B)\{1+(a_1'/a)-(b_1'/b)\}\ln\{1+(B/Z)\} \qquad (2\text{-}9)$$

where $a_1' = 2\Sigma y_i a_{1i}$ and $b_1' = 2\Sigma y_i b_{1i}$

Computer programs used to correlate the T-x relation and the prediction of y_1 are shown in Appendix F.

Chapter III

EXPERIMENTAL DETAILS

Two types of experiments were performed in this study. In one, the P-T projection of the upper branch of the three-phase solid-liquid-gas coexistence curve (Figure 2.4(b)) starting near the melting point of naphthalene and terminating near the UCEP was measured. In another, the solubility of naphthalene in supercritical carbon dioxide was measured. The P-T projection of the S-L-G coexistence curve was measured, prior to obtaining the solubility data, so that solubility behaviors such as solid-fluid and liquid-fluid equilibrium were known before the solubility measurement.

3.1 Materials.

The 99+% purity naphthalene with melting temperature of 353.15 K was supplied by the Fisher Scientific Company. Liquid carbon dioxide at ambient temperature and saturated pressure was supplied by Air Products & Chemical Inc. and the purity of carbon dioxide was 99.9+%. Acetone with minimum purity of 99.9+% was supplied by Canlab, a Division of McGraw Supply Ltd.. All these chemicals were used without further purification.

The critical properties of the two components, naphthalene and carbon dioxide, are listed in Table 3.1 whereas the pure solid properties of naphthalene are listed in Table 3.2.

Table 3.1: Critical properties of naphthalene and carbon dioxide.

(for reference, see [38])

Property	Naphthalene	Carbon dioxide
T_c [K]	748.4	304.2
P_c [MPa]	4.05	7.38
v_c [cm^3/mole]	410.0	94.0
ω	0.302	0.225

Table 3.2: Physical properties of naphthalene.

(for reference, see [39])

Property	Naphthalene
Molecular structure	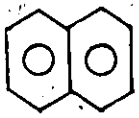
Tm [K]	353.15
v_1^s [cm^3/mole]	128.6
ΔH_f^0 [J/mole]	19060.8
Antoine coeff. *	
A	7.2144
B	2926.6
C	-35.8

* $\log P_1^{sat} = A - B/(C+T)$,

where T is in K,

and P_1^{sat} is in 10^{-1}MPa.

3.2 Measurement of the Three-Phase (Solid-Liquid-Gas) Coexistence Curve.

Various techniques for determining the P-T projection of the S-L-G coexistence curve are described in the literature. In general, these techniques can be described by the following two experimental methods.

In the first method, the P-T projection of the three-phase curve is determined by intersection of the liquid-gas (L-G) boundary and the solid-fluid (S-F) boundary in the P-T diagram at constant composition [40-41]. The composition of the mixture is measured by introducing known amounts of solid and light component into a high pressure view cell. The solid-fluid region separating from the fluid region is measured by slowly heating a mixture of solid substance and fluid phase at constant pressure until all the solid has disappeared. The liquid-gas boundary is measured by slowly increasing the pressure at constant temperature until either the liquid phase or the gas phase disappears. This method offers advantages of measuring the P-T-x-y characteristics of the S-L-G coexistence curve and the UCEP. However, a lot of experimental time is needed in this method.

The second method, the so called the "first melting point" method, is commonly used by most of the researchers [5,42] to determine the pressure and temperature of the S-L-G coexistence curve. Using this method, P-T projection of the three-phase curve is determined quickly. However, the gas-phase and liquid-phase compositions as well as the UCEP cannot be measured. In this method, starting from a solid-fluid condition, temperature is increased slowly until the solid begins to melt. This temperature is then taken as the three-phase coexistence temperature.

A different technique was used in this study to determine the P-T-x characteristics of the three-phase curve. Instead of using the "first melting point" method, the "first freezing point" method was used. This method provided a fast and reliable determination of the P-T projection as well as the liquid-phase composition of the three-phase curve. The experimental apparatus and procedure are described in the following two sections.

3.2.1 Experimental Apparatus.

The high pressure view cell along with the accessory equipments that were used to measure the temperature, pressure and liquid-phase composition are shown in Figure 3.1. The apparatus consisted of five major sections: a pressurizing system, a temperature controlled water bath, a high pressure view cell with magnetic stirring system, a solid recharging system and a composition analysis system.

In the pressurizing system, liquid carbon dioxide from a supply cylinder was pressurized by an air-operated automatic boost pump (max. 68.9 MPa, Futurecraft Corporation). A hand loader type pressure regulator was adjusted to a desired outlet pressure and the boost pump operated automatically until reaching the adjusted setting. The system pressure was measured using Dynisco pressure transducers (B2 : model 112851, max. 13.8 MPa; B1 : model 112743, max. 137.9 MPa). Both transducers were located very close to the high pressure view cell. Pressure readings were indicated by a pressure digital recorder. Both transducers were calibrated with a dead weight pressure tester (Testing Instrument Co. Inc.). The calibration curves for both transducers are shown in Appendix C. The accuracy of the pressure trans-

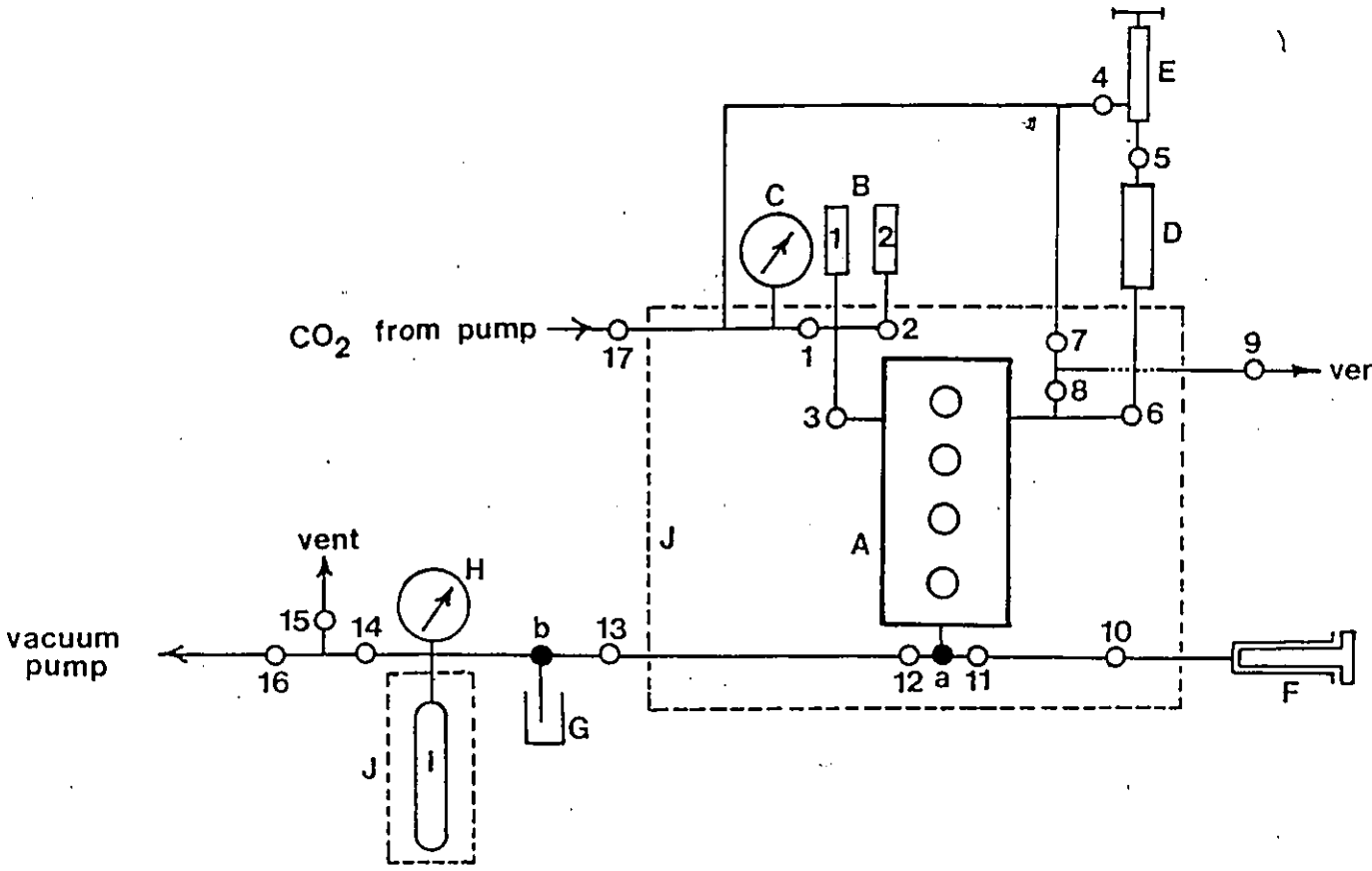

Figure 3.1: Schematic diagram of apparatus for measuring the P-T-x curve.

A : high pressure view cell,

B : pressure transducer,

C : pressure gauge, D : solid vessel,

E : hand pump, F : syringe,

G : solid sampler, H : pressure gauge,

I : sample cylinder, J : water bath,

a : three-way valve, b : three-way ball valve.

ducers (B1 and B2) was estimated to be ± 0.04 MPa and ± 0.02 MPa respectively. Pressure gauge C was used as a rough indication of pressure.

A two-layer (insulated with foam) stainless steel water bath (45cm x 45cm x 50cm) was specially designed for the purpose of this study. Polypropylene balls (Euromatics, dia. 20 mm) were used to keep water from evaporation and cut down the heat loss. These balls could withstand temperature up to 383.15 K. Temperature control was maintained using a precision temperature controller (model 250, Bayley Instrument Co.). The controller emitted pulses to provide current for a 1000 watts heater (Vycor brand, Corning 16790). A high speed stirrer was used to ensure the temperature uniformity of water bath. Temperature could be easily maintained from 328.15 to 353.15 K within ± 0.01 K. To attain a high temperature quickly, a second heater (Vycor brand, 1000 watts) powered with 110-120 V was used. A bath cooler (PBC-2, Neslab Instrument, Inc.) was used to decrease the bath temperature during the freezing point measurement. The bath temperature was measured using a Hewlett-Packard quartz thermometer (model 2801A) which was calibrated at the triple point of pure water with a platinum resistance thermometer (S.N. 1775701, calibrated 1968 IPTS scale, Leeds and Northrup). The calibration of the quartz thermometer is shown in Appendix C. Sensor (S.N. 1126-44) of the quartz thermometer was located on the outside skin of the cell. The accuracy of the temperature measurements was estimated to be ± 0.01 K. The correction factor which had to be added to each of the temperature readings, from 330.15 to 353.15 K, was 0.02.

The high pressure view cell (max. 68.9 MPa) with an internal volume of approximately 25 cm^3 was supplied by Jerguson Gauge and Valve Company. During the experiment, liquid and gas phases were mixed by the action of a magnetic stirrer (15 cm long) previously inserted into the cell. The motion of the stirrer was controlled with a doughnut-shaped magnet which was moved vertically up and down on top of the cell by a motor. A cathetometer was used to observe the crystallization of naphthalene.

The solid recharging system consisted of a hand pump (Ruska Instrument Corporation) and a solid vessel (max. 34.5 MPa) with an internal volume of approximately 50 cm^3. Heating tape was used to melt the solid naphthalene so that naphthalene could be charged into the cell using the hand pump.

The composition analysis system was designed in the following way so that the liquid-phase composition could be sampled and measured. A three-way valve (SW-2075, max. 75.8 MPa at room temp., Autoclave Engineers) was connected to the high pressure view cell as close as possible so that a saturated liquid phase could be sampled. This three-way valve, valve a in Figure 3.1, had a feature that only the way connected to the cell was opened or closed while the other two ways connected to valves 11 and 12 were always on. The sample loop between the three-way valve and these valves was cut short to about 2.5 cm each. Three long handles which extended out of the water bath were used to control the three valves. Another three-way valve (SS-41XS2, max. 17.2 MPa at 293.15 K, Whitey) was used to analyze the solid or gas phase. This three-way valve had a different feature:

the sample loop from the bath was either connected to a solid sampler (glass beaker, 200 cm^3) or to a sample cylinder (internal vol. 300 cm^3, Whitey). During the expansion process, carbon dioxide pressure released from liquid naphthalene was measured using a Bourdon-tube Heise gauge (max. 344.6 KPa, accurate to ± 0.02 KPa). The sample cylinder was immersed in a circulated water bath so that a stable temperature was maintained, as measured using the quartz thermometer described previously. Acetone from a syringe was used to dissolve the solid naphthalene deposited on the wall of the sample loop and line. The resulting solution was then forced down to the solid sampler using the syringe. In case of clogging, the sample loop and the line were heated using a heating tape. The amount of solid naphthalene collected was weighed using a micro-balance (Mettler H2O, Fisher Scientific) with an accuracy of ± 0.0001 g. Gases such as acetone, air and carbon dioxide were removed using the vacuum system which consisted of a vacuum pump and a liquid-nitrogen trap system.

3.2.2 Experimental Procedure.

Before the experiment, valves a, 4, 5, 6, 11 and 15 were closed. The high pressure view cell, initially loaded with approximately 15 grams of naphthalene, was purged of air with carbon dioxide at approximately .1 MPa through valve 9. After three to four purgings, valves 7, 8 and 9 were closed. At this moment, the sample loop between valves 11 and 12 was evacuated using the vacuum system. After the evacuation, valves 12, 13 and 16 were closed. The system was then brought to a desired pressure and maintained there for approximately 30 minutes to ensure thermal and pressure equilibrium.

Starting with a solid-fluid equilibrium in the cell, the temperature was increased until the solid naphthalene began to melt. This melting point was recorded. The system was then heated slowly until the solid was completely melted. The temperature was then maintained with rigorous stirring for approximately 30 minutes so that liquid naphthalene was saturated with carbon dioxide. Complete mixing was essential since crystallization would occur at a higher temperature if saturation was not attained during the cooling process. The saturated solution was cooled slowly so that the first freezing point was observed precisely. Conditions when the first crystal formed were measured as the three-phase coexistence point. The solid was then melted and frozen again in an effort to obtain a consistent and accurate result. In most cases, the interval between the first measurement and the second measurement was within ± 0.5 K.

The composition of the liquid naphthalene at the three-phase conditions was sampled at the second measurement of the freezing point in the following manner. When the first crystal was noticed, usually formed near the window of the view cell, the three-way valve a was opened and saturated liquid naphthalene flowed into the sample loop. Since the crystallization formed rapidly, the procedure had to be carried out very quickly. The saturated liquid phase was then expanded immediately into the loop between valve 12 and 13. Valve 13 was opened slowly so that carbon dioxide was expanded into the sample cylinder through the three-way ball valve b. The rise of pressure at the bath temperature was then corrected to the condition at 298.15 K using an ideal gas equation. A calibration curve between the rise of pressure

and the number of moles of carbon dioxide is presented in Appendix D. The amount of carbon dioxide was obtained using the calibration factor. After that, valve 11 was opened and solid naphthalene was collected by forcing acetone to the solid sampler through the three-way ball valve b.

3.3 Solubility of Solid in Compressed Carbon Dioxide.

Experimental designs for measuring the solubility of heavy components in a supercritical fluid can be classified as either static or flow systems.

For the static systems, the solubility of the heavy component in the supercritical fluid can be determined in many ways. In one method [40], a known amount of both components is introduced into a calibrated high pressure view cell. Temperature and pressure of the system are adjusted at constant composition until one of the phases disappears. In this manner, various pressures and temperatures are obtained at constant composition without sampling. P-x-y isotherms can then be deduced from these data.

In another method [2,43], a tablet of compressed solid with known weight is placed in a high pressure column. A known amount of light component is compressed into the cell. At constant temperature, the tablet is set in motion by means of a permanent magnet stirrer. After 15-20 minutes, the system is depressurized allowing the solid to precipitate from the saturated fluid phase. A soft hair brush is used to remove solid settled on the surface of the tablet. The amount of solid dissolved is determined from its weight loss, and hence its concentration in the light component is determined.

In an earlier effort of the author [44] and the work of King et al. [45], a different static technique was used to determine the solubility data. In this experiment, the light component is recirculated through the heavy component contained in a high pressure cell until equilibrium has been achieved under controlled conditions of temperature and pressure. Samples of both phases are then valved off in sample bombs and the contents are analysed by the expansion process. During the process, the contents of the sample bombs are allowed to expand gently into previously evacuated sampling vessels of known volumes. The number of moles of the light component present in each sample bomb is calculated from the pressure rise in the expansion system. The deposited heavy component during this process is washed down into a receiving vessel using a suitable volatile liquid solvent such as acetone, which is subsequently evaporated off. By knowing the weight gain of each receiving vessels, and thus the amount of heavy component, the composition of each phase is calculated. For system involving solid phase, only gas phase is sampled and analysed.

Compared with the static systems, the flow systems are easy in their operations and thus minimum experimental times are required. In general, a single-pass, continuous flow system is used in most of the study [14-18]. The heavy component is packed into high pressure columns and remains stationary throughout the experiment while a light component is compressed into the columns until that equilibrium is attained. Once saturation of the light phase is obtained, it is flashed to ambient conditions across a heated metering valve. The amount of each component is collected and measured. The main limitation of this technique is that only the light phase is sampled.

A flow system was used in this study because of its easy operating and sampling characteristics. The design was similar to the system described above with one major difference. In this design, a bypass line was installed. This offered the advantage that any loss of the solid due to holdup in the metering valve and line was avoided since carbon dioxide could be used to flash any solid lost in the valve and line to the solid sampler.

3.3.1 Experimental Apparatus.

The experimental apparatus is shown in Figure 3.2. It consists of three main sections: a pressurizing system, a temperature controlled water bath containing two high pressure columns and a composition analysis system.

The pressurizing system was basically the same as the system described previously. After setting the desired pressure, carbon dioxide was compressed by the automatic boost pump B to the buffer C. The automatic boost pump operated automatically to make up loss of pressure during the experiment. The pressure was maintained constant to within ± 1-2% of the setting. The system pressure was measured with a Bourdon-tube gauge (max. 34.5 MPa , U.S. Gauge Co.). This gauge was located before the presaturator. Since the flowrate and viscosity of the fluid were low, the pressure drop between the gauge and the metering valve was negligible. Thus system pressure indicated by the gauge was reliable.

Temperature control was maintained in a stirred water bath (35cm x 35cm x 60cm) using a precision temperature controller described previously. Polypropylene balls were used to prevent heat loss. Thus

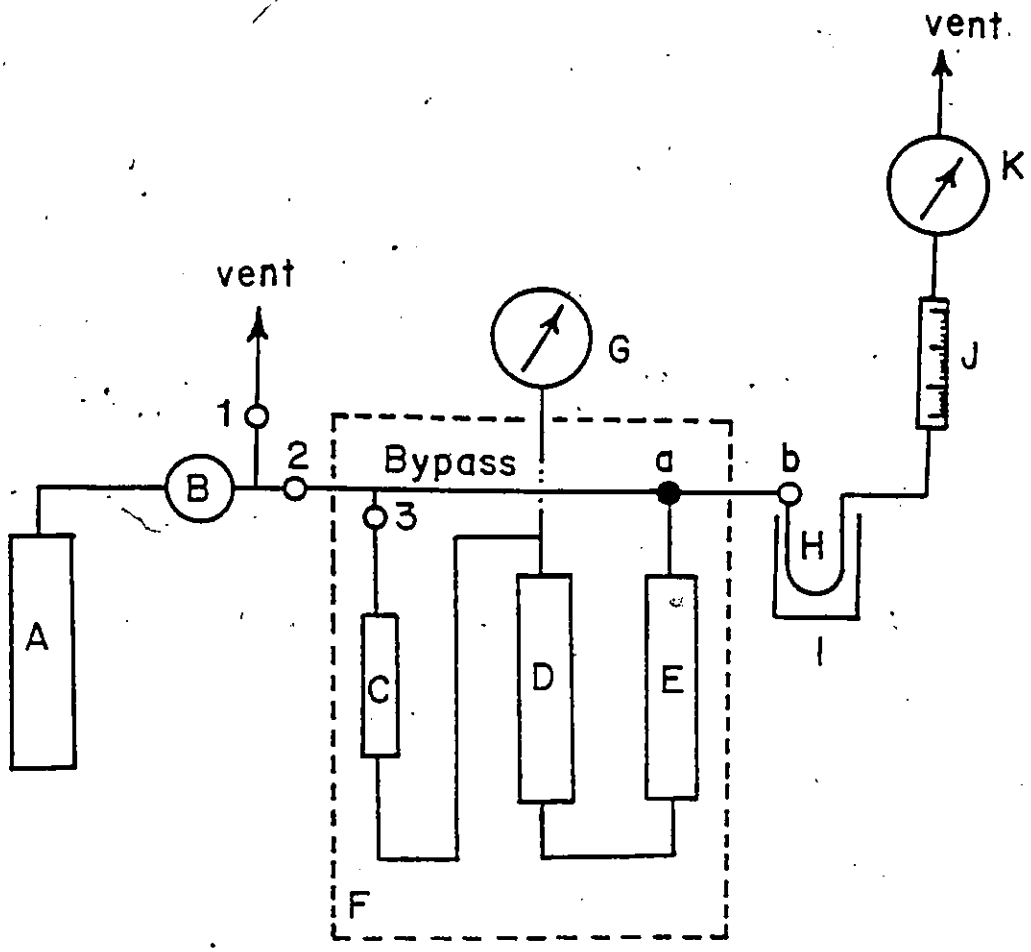

Figure 3.2: Schematic diagram of the flow system.

A : gas cylinder, B : high pressure pump,

C : buffer, D : presaturator,

E : saturator, F : water bath,

G : Bourdon-tube gauge, H : solid sampler,

I : ice bath, J : rotameter,

K : wet test meter, a : three-way valve,

b : metering valve.

temperatures were easily maintained from 308.15 to 332.15 K within ± 0.01 K. The system temperature was measured using the quartz thermometer (HP model 2801A) mentioned previously. The accuracy of the temperature measurements was estimated to be ± 0.01 K. The correction factors which had to be added to the temperature readings for 308.15 K and 332.15 K were 0.04 and 0.02 respectively.

A gas buffer volume used in this study served two purposes. It was used to bring the carbon dioxide temperature to the bath temperature. It also served as a storage reservoir so that a stable flow of carbon dioxide was maintained. Hence, fluctuation of the system pressure was minimized during the run. Two high pressure columns were connected in series so that saturation of the fluid phase was attained. The presaturator (1.3 cm I.D. by 20.8 cm, 27.6 cm^3 internal vol., 316 S.S.) had a larger volume than the saturator (1.0 cm I.D. by 20.8 cm, 16 cm^3 internal vol., 316 S.S.). These two columns were packed with a mixture of stainless steel beads and solid naphthalene. These beads were added to prevent agglomeration of the solid and channeling of the supercritical carbon dioxide. In case of a liquid-gas equilibrium, these beads were useful in increasing the contact surface area of the liquid with the gas. Glass wool was inserted at the top and bottom of each column to prevent entrainment of the solid. A three-way ball valve connecting the bypass line and the saturator was supplied by Whitey (SS-41XS2, max. 17.2 MPa at 294.15 K). At high temperature measurements, this three-way valve was replaced by another three-way valve (SW2075, max. 75.8 MPa at R.T., Autoclave Engineers) due to the melting of the Teflon packing of the valve.

The composition analysis system consisted of a metering valve, a solid sampler, a rotameter and a wet test meter. The system pressure was reduced to atmospheric pressure across the metering valve (SS-31RS4, orifice dia. 1.59 mm, Whitey). Low flowrates such as 100-200 cm^3/min. (ambient conditions) were achieved using this valve. The essential key to smooth flowrates was preventing solid precipitation around the metering valve due to Joule-Thomson cooling. Thus the metering valve and lines around it were heated to approximately 453.15 K to prevent plugging. A solid sampler (glass U-tube) plugged with glass wool was maintained at ice temperature in an ice bath to prevent entrained solid from escaping the sampler and to enhance solid precipitation. In most instances, over 99% of the solid was trapped in the U-tube. The gas flow was measured by a wet test meter (Precision Scientific Co.) connected in series with a rotameter. The rotameter was used to indicate the constant and steady flowrate while the wet test meter was used to integrate the total volume of carbon dioxide. At this point, the stream temperature was measured while the pressure was assumed to be atmospheric pressure.

3.3.2 Experimental Procedure.

After loading with solid naphthalene, the system was purged of air with carbon dioxide at approximately 1 MPa for three to four times through valve 1 (Figure 3.2). A leak test was then carried out at tank pressure (approximately 6 MPa). If no leakage was found, the columns were immersed in the water bath for one hour to obtain thermal equilibrium.

To start the experiment, valves 1, 3 and b were closed. The bypass line was opened and the saturator exit line was closed. The system was pressurized with carbon dioxide to a desired pressure. The metering valve b was then opened and adjusted slowly so that a steady and low flowrate (100-200 cm^3/min.) was attained. When a steady flowrate of carbon dioxide was obtained, valve 3 was opened allowing the carbon dioxide to flow into but not out of the columns. After that, valve 3 was closed again. The experiment was run for 20 to 30 minutes so that equilibrium was established in the columns and the distilled water in the wet test meter was saturated with carbon dioxide. During this equilibration time, the metering valve b was heated slowly. After that, the bypass line was closed in order to record the initial reading of the wet test meter. Valve 3 and the saturator exit line were opened to allow carbon dioxide to flow into the presaturator and saturator. The experiment was run for 20 to 30 minutes so that the saturated fluid phase was displaced from the presaturator and saturator to the metering valve. The metering valve and valve 3 were closed and the total volume of carbon dioxide was measured. The bypass line was then used to flash solid, which precipitated in the line and the metering valve, to the U-tube at a slow flowrate of carbon dioxide.

Chapter IV

RESULTS AND DISCUSSION

The P-T-x data of the three-phase S-L-G curve of naphthalene(1)-carbon dioxide(2) system are listed in Table 4.1. Raw data and sample calculations are shown in Appendix E. In the P-T-x experiment, we tried to measure the UCEP and liquid-gas critical locus but failed to do so. Vivid red colours were observed in both liquid and fluid phases at 26.85 MPa and 336.65 K indicating that this condition was close to the liquid-gas critical point. Since the meniscus between the liquid and fluid phase did not disappear with an increase in temperature, this condition was not at liquid-gas critical point. The main reason we could not obtain the liquid-gas critical point is that the overall composition of the mixture did not equal to the critical composition.

The P-T data obtained from this study as well as the data of McHugh [3,5] and Prins [41] are shown in Figure 4.1. The liquid-phase composition of the three-phase curve (x_1) at different temperatures predicted by the T-x correlation (shown in Figure 4.3) is also shown in Figure 4.1. McHugh used the "first melting point" method to determine the three-phase curve. In his study, the solid was alternatively frozen and melted a number of times so that the temperature interval of solid-fluid and liquid-fluid was decreased to within a small range. The temperature interval was decreased to within ± 0.5 K as

Table 4.1: P-T-x data of the three-phase curve for the naphthalene(1)-carbon dioxide(2) system.

P [MPa]	T [K]	x_1
2.07	348.79	-
2.22	348.18	-
2.84	347.30	-
3.53	345.57	-
6.69	340.25	-
8.53	337.10	-
9.55	335.26	-
10.19	334.46	0.6136
10.90	333.34	0.6473
11.54	332.99	-
12.46	332.40	-
13.30	331.73	0.4237
14.26	331.98	-
15.85	332.17	0.4296
17.59	332.34	0.3263
20.39	332.59	-
21.92	332.83	0.2824

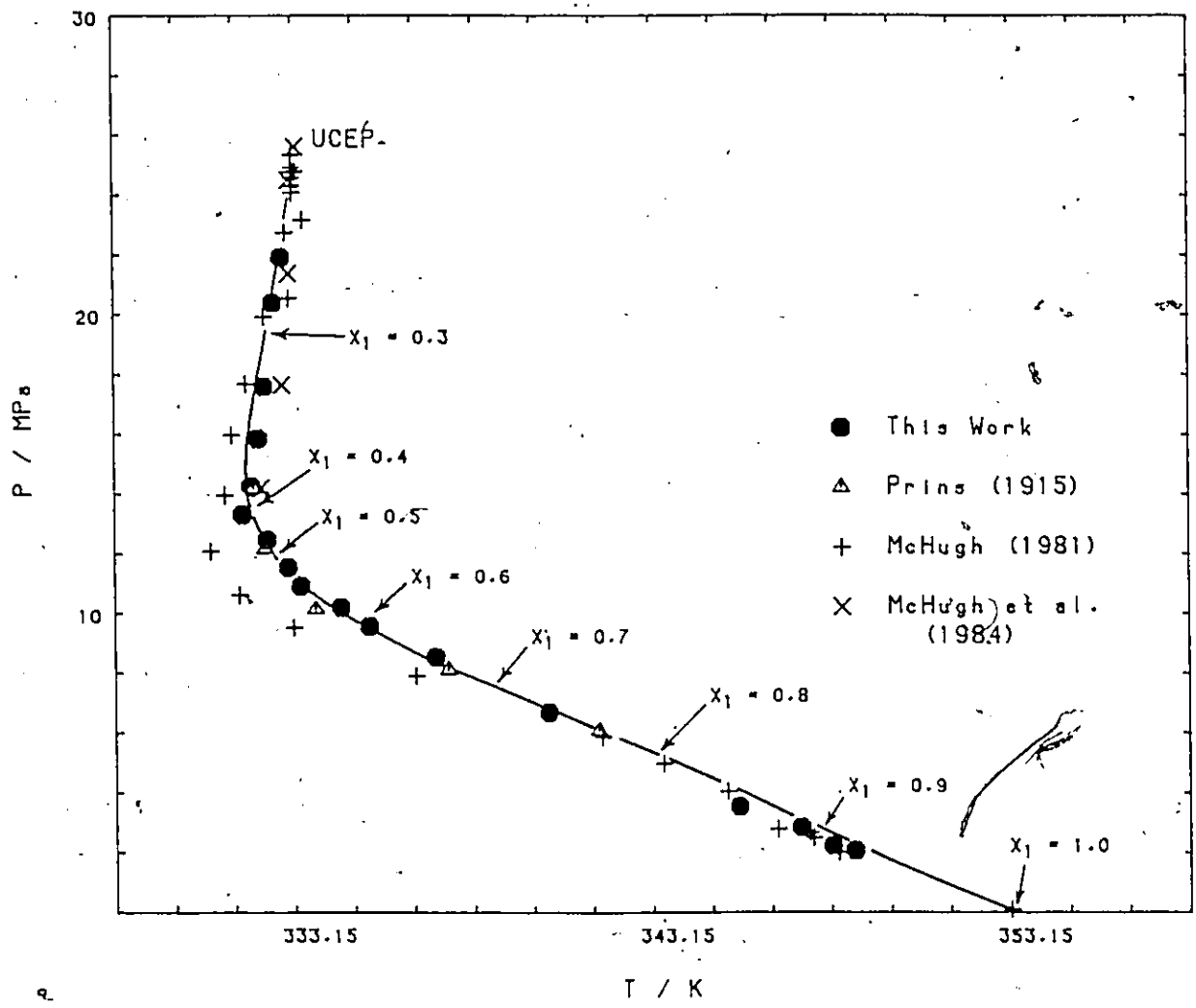

Figure 4.1: P-T projection of the naphthalene-carbon dioxide S-L-G curve.

reported in his Ph.D. thesis [5] and within ± 0.1 K in his recent work [3]. Pressure was kept to within ± 0.1 MPa. From Figure 4.1, some discrepancy between this work and his work exist and this is probably due to the following reasons. In his design, the volume of high pressure view cell was very small (internal vol. approx. 1 cm^3) compared to the volume of the Bourdon-tube Heise gauge. Since the gauge was located far from the water bath, the pressure measurement was not reliable. In the experiment, we also measured the first melting point. It was found that data measured using the "first melting point" method were scattered compared to that using the "first freezing point", as shown in Figure 4.2. This is because the moment that the solid began to melt was hard to determine. Another important reason is that the uniformity of liquid-phase concentration was not ensured when the solid began to melt because we could not stir the solid phase. This problem was eliminated using the "first freezing point" method. In the "first freezing point" method, we could mix the liquid phase rigorously so that saturation of liquid phase was ensured. Thus the "first freezing point" method was proven to be more reliable than the melting point" method.

This work agrees well with the work of Prins [41]. Prins determined the P-T projection of the three-phase curve by every intersection of the liquid-gas (L-G) boundary and the solid-fluid (S-F) boundary (see Section 3.2). Thus this method was reliable although he did not report the accuracy of data. Hence the technique used in this study is reliable.

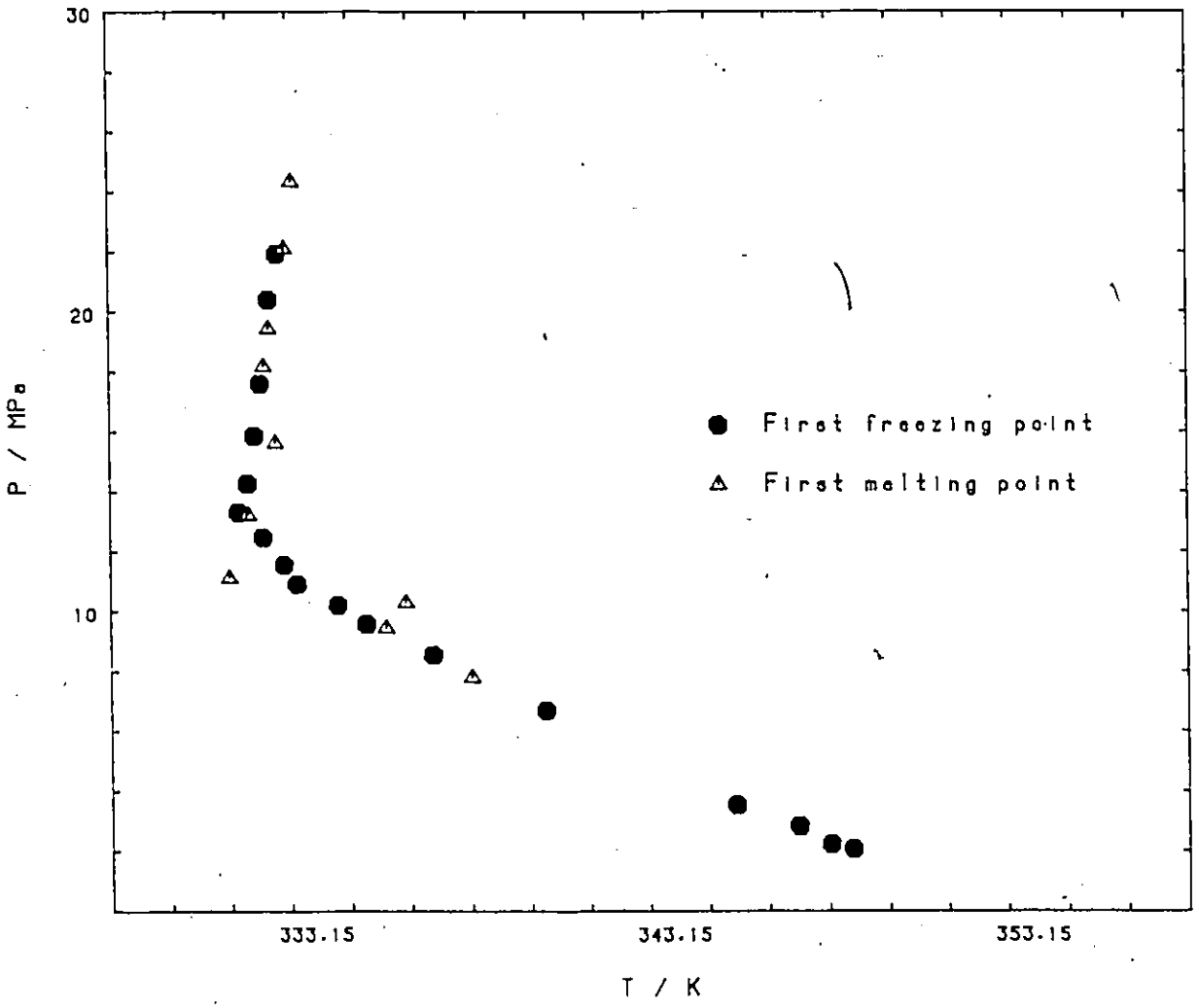

Figure 4.2: Comparison of the "first melting point" method with the "first freezing point" method.

The T-x projection of the three-phase line is shown in Figure 4.3. In the figure, some scattered x_1 data are omitted. It was very difficult to obtain x_1 data because the saturated liquid phase solidified easily during the sampling process. Also, the x_1 data were more scattered in the high temperature region, i.e. near the pure solid region (see Figure 4.3). In this region, sampling was extremely difficult because the liquid phase solidified very quickly due to the low concentration of carbon dioxide in the liquid phase.

Correlation of T-x projection by eq.(2-1) as well as the projection of the ideal solution are shown in Figure 4.3. The van Laar equation, eq.(2-3), used to estimate γ_1 is shown in Figure 4.4. Experimental γ_1 values were calculated from eq.(2-1) using the experimental T and x_1 data. The best fitted values of A_{12} and A_{21} were 3.228 and 1.372 respectively by minimizing the sum of squares of the difference between experimental and calculated γ_1 values. From Figure 4.3, the T-x projection of the three-phase line is well correlated by eq.(2-1) although several assumptions are involved. At low concentration of carbon dioxide, T-x projection and the ideal projection merge since the liquid naphthalene behaves like an ideal solution at the low concentration region. As the concentration of carbon dioxide increases, the T-x projection deviates more from the projection of the ideal solution. In this system, positive deviation was found because the activity coefficient was positive.

The solubility data for naphthalene in supercritical carbon dioxide as well as the enhancement factor at 308.15 K and 332.15 K are listed in Table 4.2 and Table 4.3 respectively. Raw data and sample calcula-

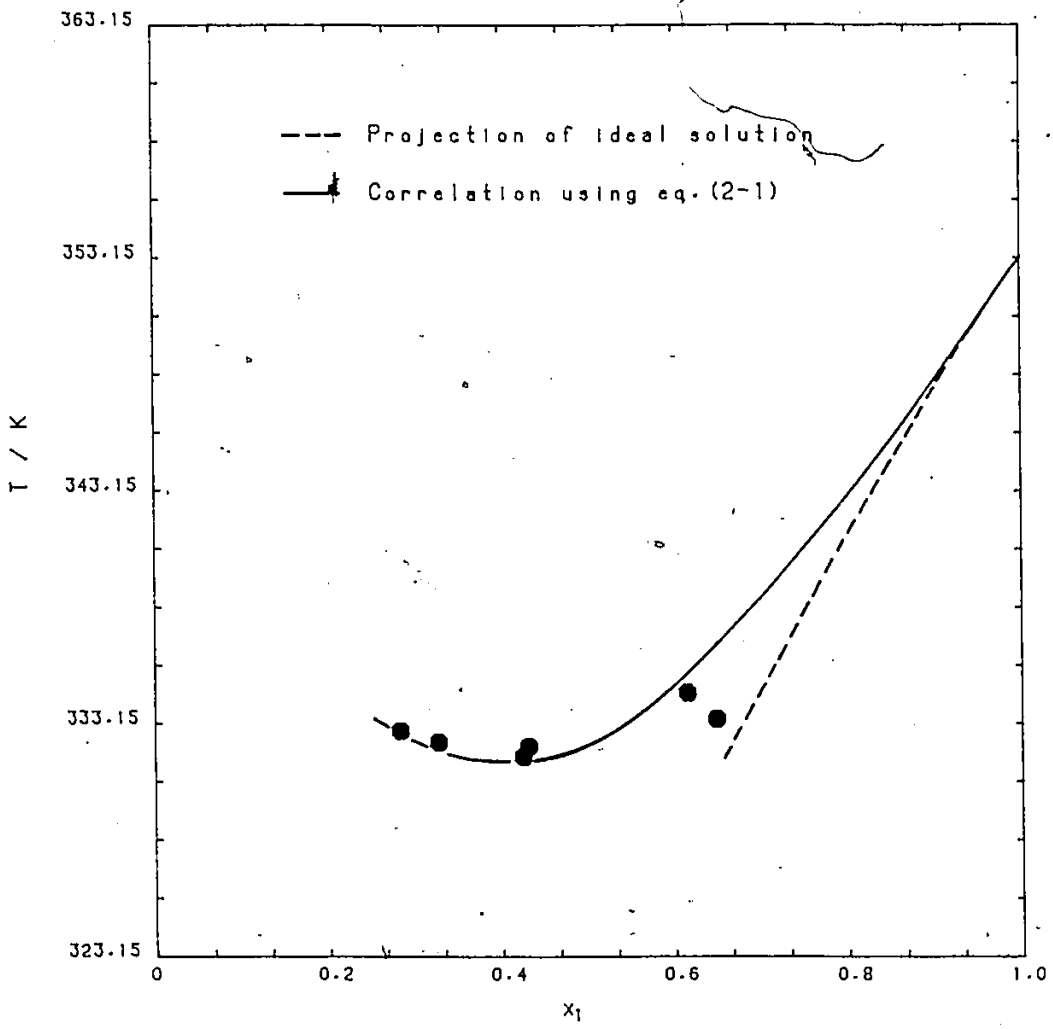

Figure 4.3: T-x projection of the naphthalene(1)-carbon dioxide(2) S-L-G curve.

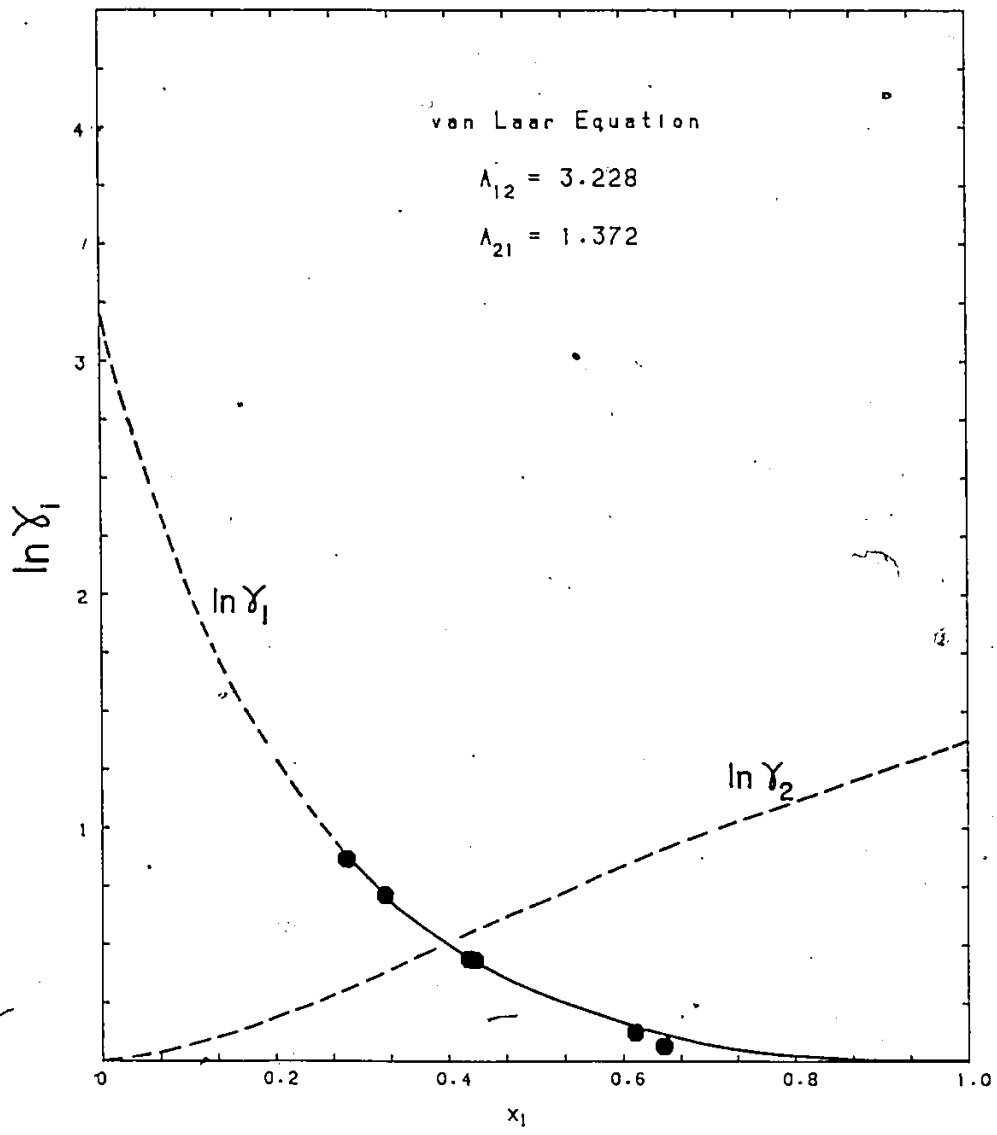

Figure 4.4: Plot of experimental γ_1 data and the van Laar equations.

Table 4.2: Mole fraction and enhancement factor of naphthalene(1) in supercritical carbon dioxide(2) at 308.15 K.

P_1^{sat} [MPa]	P [MPa]	y_1	Py_1/P_1^{sat}
2.94×10^{-4}	7.82	0.00117	3.11×10^2
	8.48	0.00690	1.99×10^3
	9.93	0.00992	3.35×10^3
	10.65	0.01114	4.03×10^3
	11.27	0.01185	4.54×10^3
	12.65	0.01271	5.46×10^3
	14.09	0.01435	6.87×10^3
	15.17	0.01537	7.92×10^3
	16.30	0.01580	8.76×10^3
	17.24	0.01639	9.60×10^3
	20.78	0.01742	1.23×10^4
	23.88	0.01841	1.49×10^4
	28.36	0.01895	1.83×10^4
	32.49	0.01944	2.15×10^4

Table 4.3: Mole fraction and enhancement factor of naphthalene(1) in supercritical carbon dioxide(2) at 332.15 K.

p_1^{sat} [MPa]	P [MPa]	y_1	Py_1/p_1^{sat}
2.18×10^{-3}	8.44	0.00131	5.08×10^{1}
	10.20	0.00251	1.18×10^{2}
	11.89	0.00633	3.45×10^{2}
	12.50	0.00831	4.77×10^{2}
	13.06 *	0.01089	6.53×10^{2}
	15.13 *	0.02562	1.78×10^{3}
	16.78 *	0.03744	2.88×10^{3}
	20.44	0.06276	5.89×10^{3}
	22.16	0.06947	7.07×10^{3}
	26.02	0.07444	8.89×10^{3}
	29.74	0.08063	1.10×10^{4}

* liquid-gas equilibrium

tion are shown in Appendix E. At 308.15 K, the reported data could be reproduced to within ± 3-5% in most instances. At 332.15 K, each solubility data was measured in a single run.

The enhancement factors for the two isotherms are plotted as a function of pressure in Figure 4.5. These factors are generally in the order of 10^3 to 10^4. In general, the relationship between the enhancement factor and pressure is approximately linear at high pressure. Temperature, however, has a negative effect on the enhancement factor.

In Figure 4.6, the solubility data at 308.15 K are compared with the work of Tsekhanskaya et al. [2] and the work of McHugh [5]. From the figure, the data obtained in this study generally agree well with the literature values indicating that equilibrium data are obtained. Thus the flow system used in this study is reliable.

Correlations using the SRK equation and two mixing rules are also shown in Figure 4.6. The optimized k_{12} value is 0.10967 using the one-parameter random mixing rules. This value is reasonable for heavy hydrocarbons-carbon dioxide system. Using the two-parameter random mixing rules, the optimized k_{12} and l_{12} values are 0.06790 and -0.07992 respectively. From Figure 4.6, the two-parameter random mixing rules (AAD = 0.5527×10^{-3} and AAD% = 10.588% from Appendix B) correlate the solubility data much better than the one-parameter random mixing rules (AAD = 1.2498×10^{-3} and AAD% = 18.914% from Appendix B). Correlations of other hydrocarbons-carbon dioxide systems show the same results (see Appendix B). This shows that the binary parameter l_{12} in the b term is more effective than the k_{12} in correlating the system containing large and small molecules.

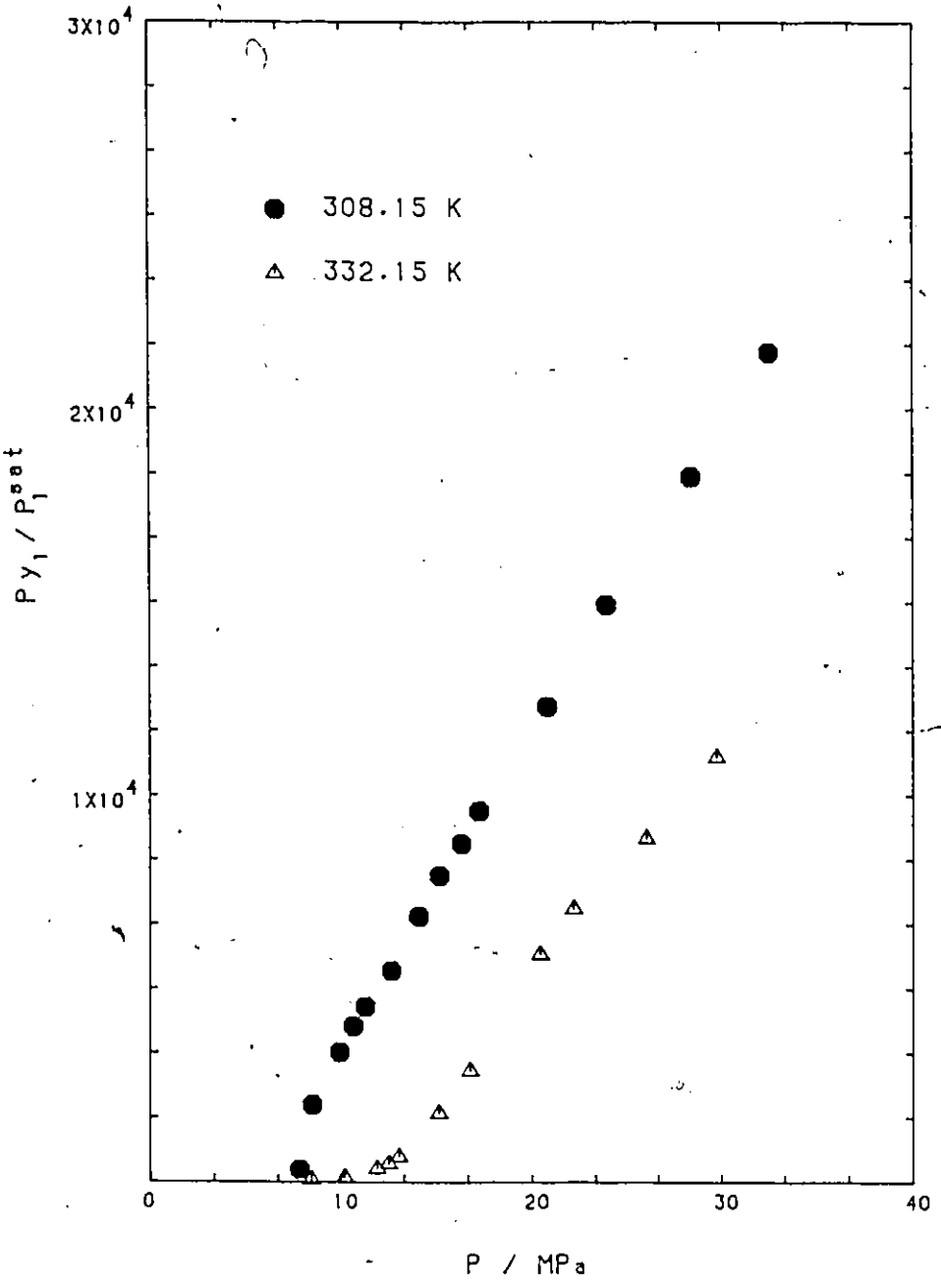

Figure 4.5: Plot of enhancement factor as a function of pressure.

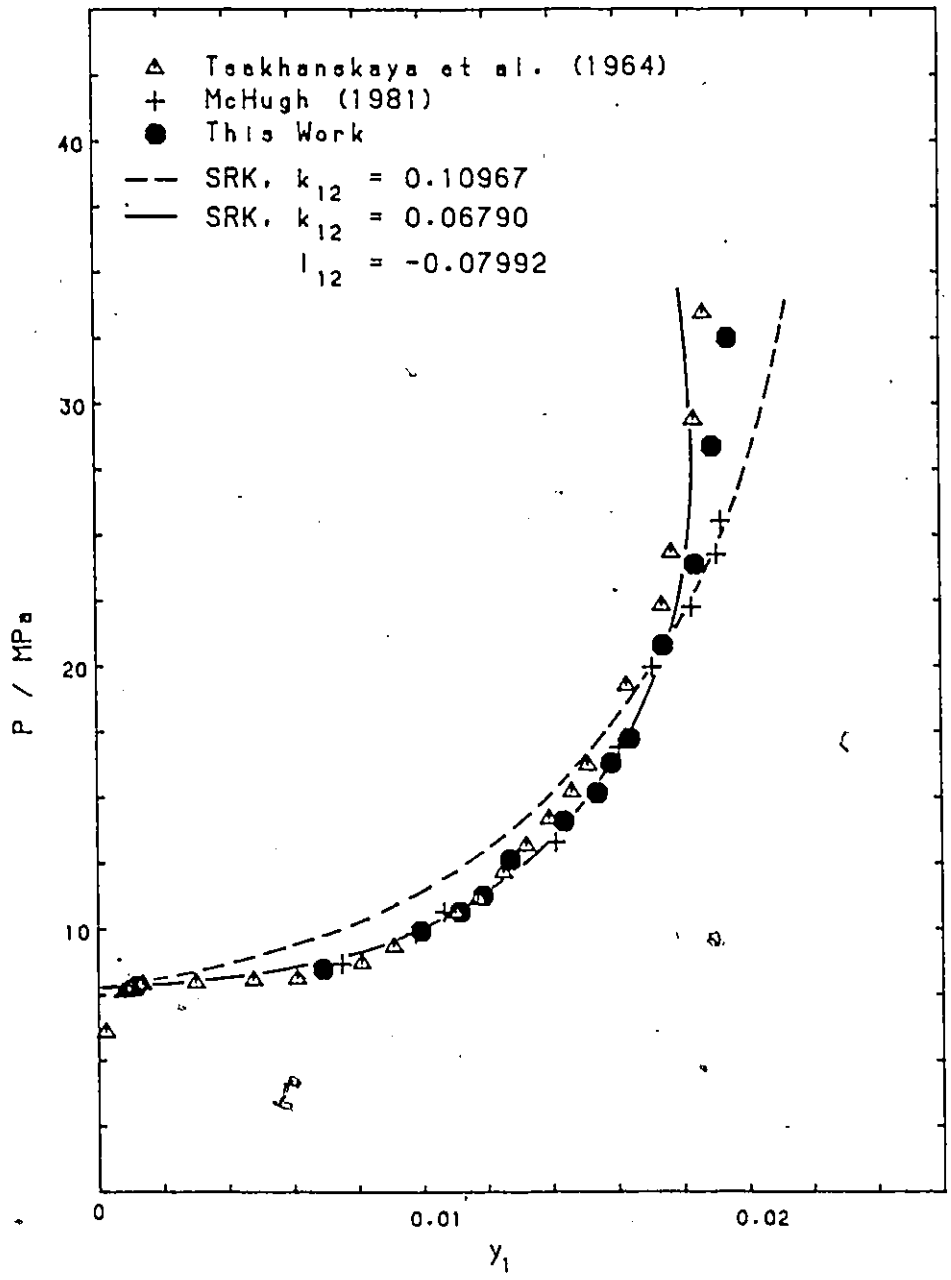

Figure 4.6: Solubility data for the naphthalene(1)-carbon dioxide(2) system at 308.15 K.

Solubility behavior of naphthalene-carbon dioxide system at 308.15 K can be quantitatively explained by the phase diagrams described in Chapter II. The LCEP was found by Prins [41] at 307.15 K and 7.6 MPa. Thus the temperature of the solubility data at 308.15 K is slightly higher than the LCEP temperature but still very close to the critical temperature of pure carbon dioxide (304.2 K). The solubility behavior at this temperature is therefore the same as the one described in Figure 2.6(b). At this isotherm, the observed solubility increases dramatically for a small change in pressure at pressure slightly higher than the critical pressure of carbon dioxide (7.38 MPa) as shown in Figure 4.6. At higher pressures, carbon dioxide is less compressible and a limiting solubility value of approximately 2 mole % is quickly attained.

The solubility data at 332.15 K are shown in Figure 4.7. The phase behavior of this isotherm is of the type shown in Figure 2.7(a) since the three-phase curve of Figure 4.1 is intersected twice at 332.15 K. In the experiment, we tried to measure the liquid phase of solid-liquid loop but failed to do so due to the limitation of the flow system (see Section 3.3). From Figure 4.1, solubility data measured from 12.7 MPa to 17.0 MPa represent liquid-gas equilibrium; but not solid-gas (or fluid) equilibrium. This solubility phase behavior could not visually observed because neither columns had a view window. However, they could be deduced from Figure 4.1. The liquid-phase compositions of naphthalene at these two pressures were estimated to be 0.484 and 0.320 respectively from Figure 4.3.

In Figure 4.7, the one-parameter random mixing rules cannot correlate the 332.15 K solubility data very well. Although the two-parameter

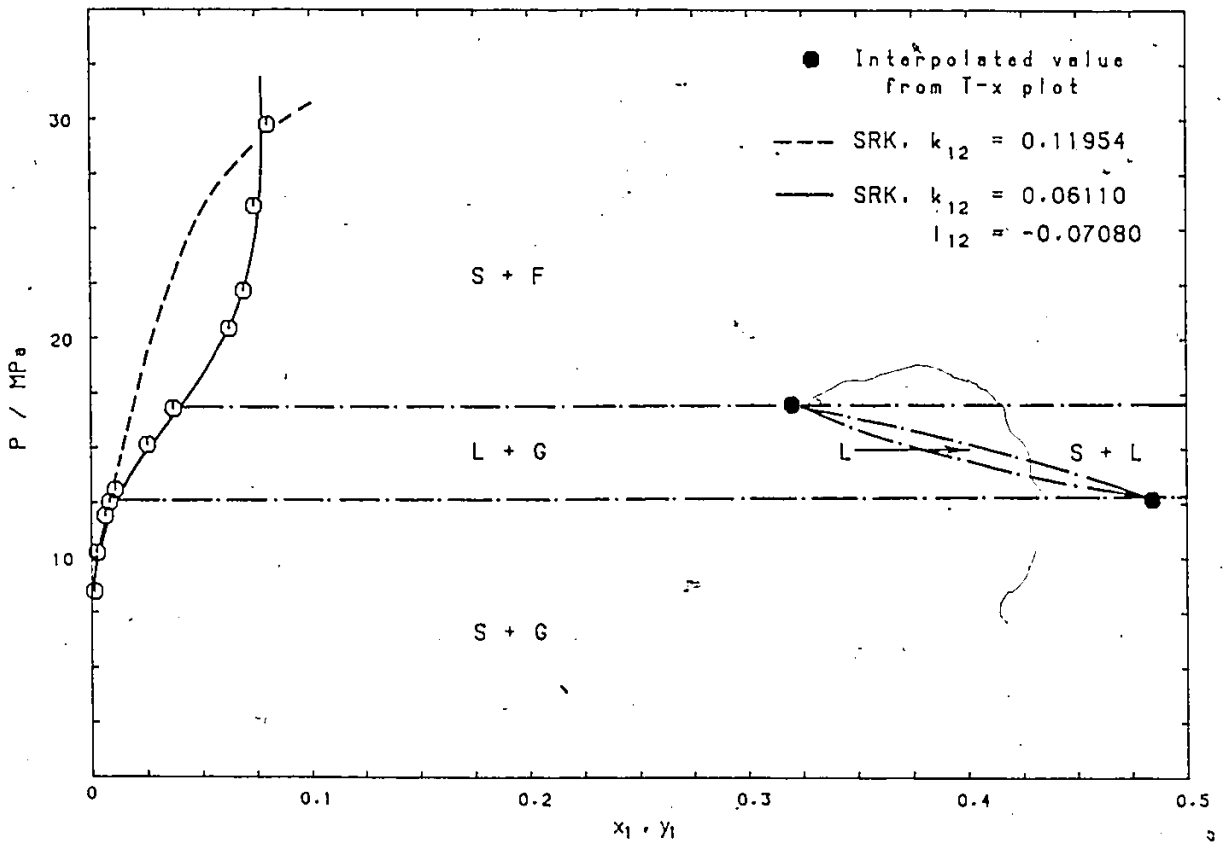

Figure 4.7: Solubility data for the naphthalene(1)-carbon dioxide(2) system at 332.15 K.

random mixing rules can correlate well with the solubility data at 332.15 K, they fail to predict the liquid-gas and solid-liquid loops. Only solid-gas (or fluid) loop is predicted using the SRK equation and these mixing rules. Although Chai [24] could predict these solubility behavior using the Peng-Robinson (PR) equation of state with modifications in the a and b terms of the heavy component, only fair agreement was obtained compared with the experimental data. Thus equation of state and random mixing rules still are not adequate for mixtures containing large and small molecules at this region.

The UCEP was found by McHugh et al. [3] at 25.6 MPa and 333.25 K. Thus the 332.15 K isotherm is slightly lower than the UCEP temperature and is higher than the temperature minimum (331.73 K from Table 4.1). The solubility behavior and loading power of this isotherm are quite different from the 308.15 K isotherm. At this temperature and at pressure near the critical pressure of pure carbon dioxide, the solubility is much less sensitive to pressure compared with the 308.15 K isotherm. At higher pressure (near the UCEP pressure) where carbon dioxide is compressed to liquid-like densities, a higher solubility is attained compared with the 308.15 K isotherm. This is due to the increased sublimation pressure of solid naphthalene at this temperature. However, as the pressure is increased above the UCEP pressure (25.6 MPa), the solubility quickly attains a limiting value of approximately 8 mole % (see solid line of Figure 4.7).

From the two isotherms, it was found that measuring the solubility data alone was not enough to study the high-pressure phase behavior. If the solubility data for 308.15 K and 332.15 K were collapsed onto a

single P-y diagram, they could represent the solubility data for the class II(A) systems (Figure 2.6). Hence, the subtle differences in the phase behavior of class II(B) systems from class II(A) systems are not apparent from inspection of the solubility data. Therefore it is absolutely necessary to determine the P-T projection of the three-phase S-L-G curve to correctly interpret the solubility data.

Finally, a three-dimensional P-T-x-y space model for the naphthalene(1)-carbon dioxide(2) system was constructed using the experimental data of P-T-x and P-y isotherms. In Figure 4.8, the P-T-x-y space model for the naphthalene(1)-carbon dioxide(2) system was constructed around the triple point of naphthalene. This three-dimensional space model is particularly useful in studying the phase behavior. For example, the P-x-y isotherm at 332.15 K can be represented by the isotherm at T_1 shown in Figure 4.8.

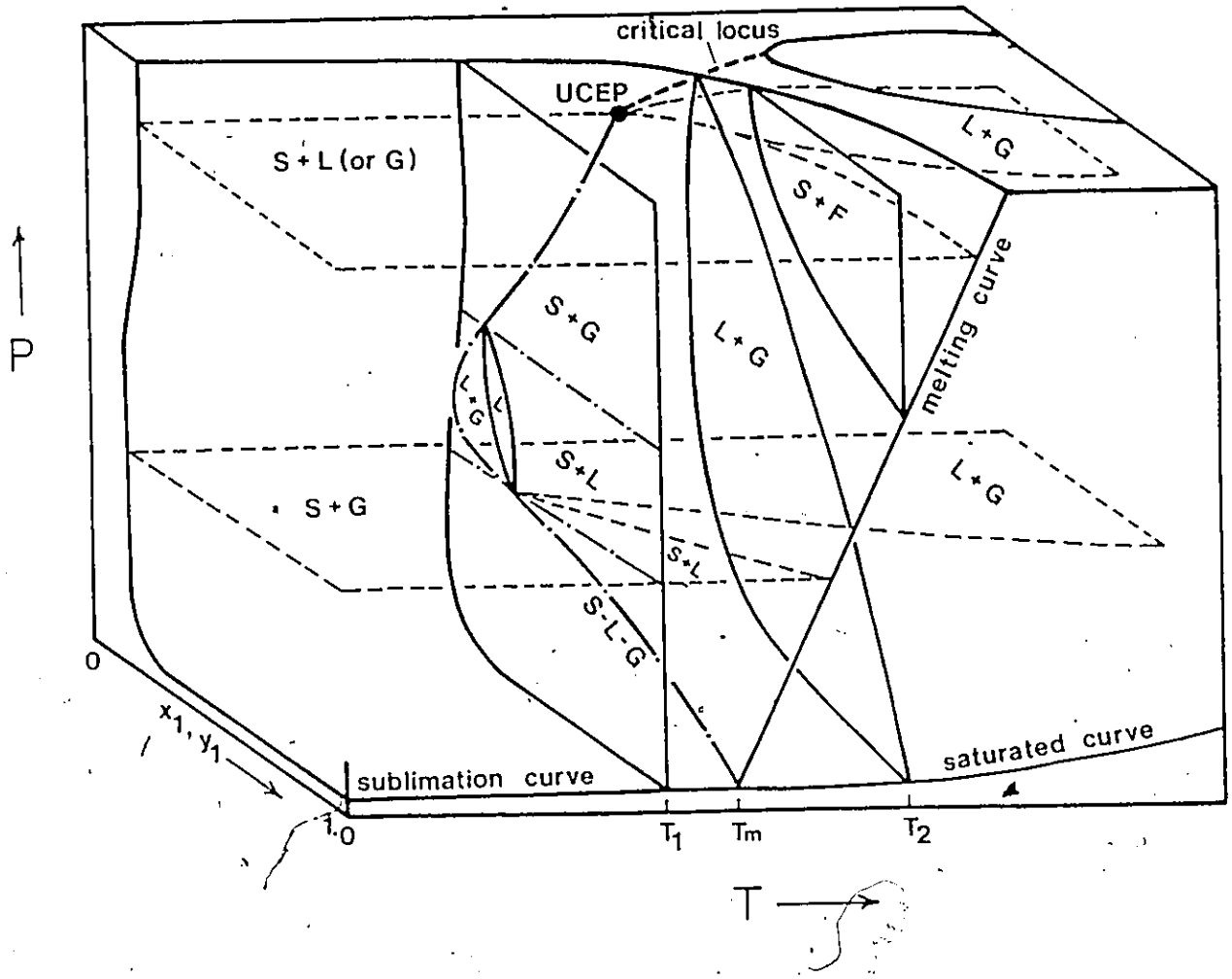

Figure 4.8: P-T-x-y space model for the naphthalene(1)-carbon dioxide(2) system around the triple point of naphthalene.

Chapter V

CONCLUSIONS AND RECOMMENDATIONS

The "first freezing point" method used in this study to determine the P-T projection of the three-phase S-L-G coexistence curve was adequate and reliable. It was found that the P-T data using the "first melting point" method were scattered. Although the measured x data are scattered in some cases, these data are very important in correlating the T-x relation. The flow system designed in this study could measure reliable and accurate solubility data although it failed to measure the liquid phase of the liquid-gas loop and the solid-liquid loop. It was found that only the gas or fluid phase, i.e. the rightmost branch of Figure 2.7(a), could be measured.

As found by McHugh [5], the naphthalene-carbon dioxide system exhibited a temperature minimum in the P-T projection of the three-phase S-L-G curve. Thus the solubility behavior of this system around the UCEP temperature was significantly different from a system without a temperature minimum. Since the different types of possible phase behavior are not distinguishable from the solubility data alone, one needs to determine the P-T projection of the three-phase line first to correctly interpret the phase behavior.

Thermodynamic modelling of T-x relation used in this study is useful in predicting the liquid-phase composition of the three-phase line. By a fast and reliable estimate of the liquid-phase composition, one can

easily locate the liquid loop of the isotherm around the UCEP temperature (Figure 2.7(a)). However, extrapolation of the T-x relation using eq.(2-1) was avoided in this study due to the lack of experimental data. Correlation of solubility data using the SRK equation of state showed that the two-parameter random mixing rules were more effective than the one-parameter random mixing rules. However, the complicated phase behavior of the 332.15 K isotherm could not be predicted by the SRK equation and these mixing rules. This is probably due to the problems of characterizing the dense gas state as well as formulating appropriate mixing rules for the highly asymmetric mixtures.

The utilization of the phase behavior in the supercritical region, especially near the UCEP region, for engineering applications depends on our level of understanding. It is recommended that more experimental data around the UCEP region be obtained. This experimental information is especially important in order to correctly apply thermodynamic models to characterize and predict the solubility behavior. Using the high pressure view cell, the entire solubility isotherm such as the one depicted in Figure 2.7(a) can be visually determined. Supercritical fluid chromatography (SFC) is recommended in measuring the fluid phase or liquid phase since the system can be sampled without disturbing the equilibrium condition. It is also suggested that other new supercritical solvent be studied in an effort to find a solvent with higher loading power and to find different type of phase behavior. Finally, experiments involving entrainer effect and mixed solvent are also recommended for future study.

BIBLIOGRAPHY

1. Diepen, G.A.M. and Scheffer, F.E.C., J. Phys. Chem., 57, 575 (1953).
2. Tsekhanskaya, Y.V., Iomtev, M.B. and Muskina, E.V., Russ. J. Phys. Chem.(Engl. Transl), 38, 1173 (1964).
3. McHugh, M.A. and Yogan, T.J., J. Chem. Eng. Data, 29, 112 (1984).
4. Krukonis, V.J., McHugh, M.A. and Secker, A.J., J. Phys. Chem., 88, 2687 (1984).,
5. McHugh, M.A., Ph.D. thesis, University of Delaware (1981).
6. S. Peter and G. Brunner, Angew. Chem. Int. Ed. Engl., 738, 10 (1978).
7. Bartle K.D., Martin, T.G. and Williams, D.F., Fuel, 54, 226 (1975).
8. Zosel, K., "Extraction with Supercritical Gases", p.1, ed. by G.M. Schneider, E. Stahl and G. Wilke, Verlag Chemie (1980).
9. Gearhart, J.A. and Garwin, L., Hydrocarbon Process, 55, 125 (May, 1976).
10. Knebel, A. H. and Rhodes, D. E., "Critical Solvent De-Ashing of Liquefied Coal", presented at 71st Annual Meeting AIChE, Miami, Florida, Nov. 1978.
11. Gouw, T.H. and Jentoft, R.E., J. Chromatog., 68, 303 (1972).

12. Basta, N. and McQueen S., Chem. Eng., p.14, McGraw-Hill (Feb. 4, 1985).

13. Mulliken, C.A. and Sandler, S.I., Ind. Eng. Chem. Process Des. Dev., 19, 709 (1980).

14. McHugh, M.A., Seckner, A.J. and Yogan, T.J., Ind. Eng. Chem. Fundam., 23, 493 (1984).

15. van Leer, R.A. and Paulaitis, M.E., J. Chem. Eng. Data, 25, 257 (1980).

16. Johnston, K.P. and Eckert, C.A., AIChE J., 27, 773 (1981).

17. McHugh, M.A. and Paulaitis, M.E., J. Chem. Eng. Data, 25, 326 (1980).

18. Johnston, K.P., Zlger, D.H. and Eckert, C.A., Ind. Eng. Chem. Fundam., 21, 191 (1982).

19. Chrastil, J., J. Phys. Chem., 86, 3016 (1982).

20. Kurnik, R.T., Holla, S.J. and Reid, R.C., J. Chem. Eng. Data, 26, 47 (1981).

21. Schneider, G.M., Adv. Chem. Phys., 17, 1 (1970).

22. Schneider, G.M., "Chemical Thermodynamics, Specialist Periodical Reports", vol. 2, chap. 4, Chemical Society, London (1978).

23. Schneider, G.M., Angew. Chem. Int. Ed. Engl., 17, 716 (1978).

24. Chai, C.P., Ph.D. thesis, University of Delaware (1981).

25. Tiffin, D.L., DeVera, A.L., Luks, K.D. and Kohn, J.P., J. Chem. Eng. Data, 23, 45 (1978).

26. Leder, F. and Irani, C.A., J. Chem. Eng. Data, 20, 323 (1975).

27. Kulkarni, A.A., Luks, K.D. and Kohn, J.P., J. Chem. Eng. Data, 19, 349 (1974).

28. Huie, N.C., Luks, K.D. and Kohn, J.P., J. Chem. Eng. Data, 18, 311 (1973).

29. Rowlinson, J.S. and Richardson, J.M., Adv. Chem. Phys., 2, 85 (1959).

30. Street, W.B., "Chemical Engineering at Supercritical Fluid Conditions", chap. 1, ed. by M.E. Paulaitis, J.M.L. Penninger, R.D. Gray, Jr., P. Davidson, Ann Arbor Science (1983).

31. Van Welie, G.S.A. and Diepen, G.A.M., J. Rec. Trav. Chim., 80, 673 (1961).

32. Czubryt, J.J., Myers, M.N. and Giddings, J.C., J. Phys. Chem., 74, 4260 (1970).

33. Kurnik, R.T. and Reid, R.C., AIChE J., 27, 861 (1981).

34. Rowlinson, J.S., "Liquids and Liquid Mixtures", 2nd. ed., chap. 6, Butterworths, London (1969).

35. Prausnitz, J.M., "Molecular Thermodynamics of Fluid Phase Equilibria", chap. 5, Prentice-Hall, Englewood Cliffs, N.J. (1969).

36. Soave, G., Chem. Eng. Sci., 27, 1197 (1972).

37. Redlich, O. and Kwong, J.N.S., Chem. Rev., 44, 233 (1949).

38. Reid, R.C., Prausnitz, J.M. and Sherwood, T.K., "The Properties of Gases and Liquids", 3rd. ed., McGraw-Hill, New York (1977).

39. Zlger, D.H. and Eckert, C.A., Ind. Eng. Chem. Pro. Des. Dev., 22, 582 (1983).

40. Van Welie, G.S.A. and Diepen, G.A.M., Rec. Trav. Chim., 80, 659, 666, 673 (1961).

41. Prins, A., Proc. Acad. Sci. Amsterdam, 17, 1095 (1915).

42. Van Gunst, C.A., Scheffer, F.E.C. and Diepen, G.A.M., J. Phys. Chem., 57, 578 (1953).

43. Tsekhanskaya, Y.V., Iomtev, M.B. and Mushkina, E.V., Russ. J. Phys. Chem., 36, 1177 (1962).

44. Cheong, P.L., B.A.Sc. thesis, University of Ottawa (1983).

45. King, M.B. and Bott, T.R., "Separation Science and Technology", 17(1), 119 (1982).

Appendix A

DERIVATION OF T-X RELATION OF SOLID-LIQUID-GAS COEXISTENCE CURVE

For a binary system in which a solid phase is in equilibrium with a liquid phase at constant T, the conditions of equilibrium expressed in terms of chemical potentials are as follows:

$$\mu_1^{0S}(T,P) + RT\ln x_1^S \gamma_1^S(T,P,x) = \mu_1^{0\ell}(T,P) + RT\ln x_1^\ell \gamma_1^\ell(T,P,x) \qquad (A\text{-}1)$$

In eq.(A-1), μ_1^{0S} is the chemical potential of pure solid 1, $\mu_1^{0\ell}$ is the chemical potential of pure liquid 1, x_1^S and x_1^ℓ are the mole fraction of component 1 in solid and liquid phase respectively, γ_1^S and γ_1^ℓ are the activity coefficient of component 1 in solid and liquid phase respectively. At the melting point of solid 1, the Gibbs free energy change is as follows:

$$\Delta G_f^0(T,P) = \mu_1^{0\ell} - \mu_1^{0S} = \Delta H_f - T\Delta S_f \qquad (A\text{-}2)$$

The entropy of fusion can be related by the following expression:

$$\Delta S_f = \Delta H_f / T \qquad (A\text{-}3)$$

Assuming ΔG_f^0 is independent of pressure , ΔH_f is equal to ΔH_f^0 and ΔS_f is equal to ΔS_f^0 (i.e. specific heat difference between the liquid and solid naphthalene, ΔCp, is assumed to be zero), the following expression can be obtained from eqs.(A-2) and (A-3):

$$\Delta G_f^0 = \Delta H_f^0(1-T/Tm) \qquad \text{(A-4)}$$

The above assumptions are made because pressure effect on the ΔG_f^0 is unknown and both ΔCp and temperature interval involved are small. Using eqs.(A-1), (A-2) and (A-4), the following expression is obtained:

$$\ln\{(x_1^{\ell}\gamma_1^{\ell})/(x_1^{S}\gamma_1^{S})\} = -(\Delta H_f^0/R)(1/T-1/Tm) \qquad \text{(A-5)}$$

For pure solid, the activity (i.e. $x_1^S\gamma_1^S$) can be assumed to be unity. Thus the temperature and liquid-phase composition can be related as follows:

$$\ln x_1^{\ell}\gamma_1^{\ell} = -(\Delta H_f^0/R)(1/T-1/Tm) \qquad \text{(A-6)}$$

Appendix B

CORRELATION METHOD FOR SOLID-FLUID EQUILIBRIUM

The solubility of heavy, nonvolatile component 1 in a supercritical component 2 is determined from standard thermodynamic relationships by equating the solid-phase and fluid-phase fugacities for the heavy component,

$$f_1^s = f_1^g \tag{B-1}$$

For the supercritical fluid phase, the binary mixture is not far removed from its critical point and contains components that are very dissimilar in molecular nature. The supercritical fluid is treated as a highly compressed gas and the fluid-phase fugacity is determined from volumetric properties,

$$f_1^g = y_1 \phi_1 P \tag{B-2}$$

By assuming the solid is pure, the solid-phase fugacity is found by Prausnitz [35] as follows:

$$f_1^s = \phi_1^{sat} P_1^{sat} \exp \int_{P_1^{sat}}^{P} (v_1^s/RT) dP \tag{B-3}$$

By substituting eqs.(B-2) and (B-3) into eq.(B-1), the thermodynamic relationship related to the mole fraction of a solid dissolved in fluid phase is as follows:

$$y_1 = (P_1^{sat}/P)(\phi_1^{sat}/\phi_1)\exp \int_{P_1^{sat}}^{P} (v_1^s/RT)dP \qquad (B\text{-}4)$$

Since P_1^{sat} is very small, ϕ_1^{sat} can be assumed to be unity. If the solid is considered to be incompressible, i.e. v_1^s is constant, then eq.(B-4) becomes

$$y_1 = (P_1^{sat}/P)(1/\phi_1)\exp\{(v_1^s/RT)(P-P_1^{sat})\} \qquad (B\text{-}5)$$

Computer program used to predict y_1 is shown in Appendix F. A number of solids-carbon dioxide systems were used to compare the two random mixing rules. The results are shown in Table B.1 and Table B.2. In the tables, solids are denoted as follows: 1 = naphthalene, 2 = phenanthrene, 3 = anthracene, 4 = fluorene, 5 = pyrene, 6 = biphenyl, 7 = triphenylmethane, 8 = hexamethylbenzene, 9 = hexachloroethane, 10 = 2,3-dimethylnaphthalene, 11 = 2,6-dimethylnaphthalene. Also, AAD and AAD% represent average absolute deviation and average absolute deviation in percentage respectively,

$$AAD = (1/N)\Sigma|y_{exp}-y_{cal}|_i$$

$$AAD\% = (1/N)\Sigma|(y_{exp}-y_{cal})/y_{exp}|_i \times 100\%$$

Table B.1: Solid-fluid correlation using the SRK equation and the 1-parameter random mixing rules.

Solid	T[K]	N	k_{12}	AAD	AAD%
1				(10^3)	
	308.15	31	0.10968	1.2498	18.914
	318.15	20	0.11010	1.9768	29.672
	328.15	38	0.11321	5.5852	32.723
2				(10^4)	
	318.00	5	0.12529	1.0778	7.871
	328.00	5	0.12511	0.8313	6.706
	338.00	5	0.12620	0.3339	7.723
	303.15	8	0.12983	1.5362	13.182
	323.15	6	0.12231	1.6806	14.506
	343.15	7	0.13413	1.3670	38.625
3				(10^4)	
	303.15	4	0.14165	0.2094	45.904
	323.15	10	0.13326	0.2065	50.527
	343.15	9	0.11322	0.1880	16.280
4				(10^3)	
	303.15	7	0.11412	0.3078	16.402
	308.15	6	0.11005	0.2684	12.884
	323.15	9	0.10690	0.2289	11.465
	343.15	8	0.09603	0.4667	13.354
5				(10^4)	
	308.15	7	0.11908	0.6084	28.435
	323.15	7	0.10824	0.7103	27.696
	343.15	8	0.08765	0.8138	48.993
6				(10^2)	
	308.95	8	0.08580	0.1961	16.570
	318.55	8	0.08261	0.2281	11.088
	322.65	8	0.08150	0.2753	10.384

Table B.1 (cont'd)

Solid	T[K]	N	k_{12}	AAD	AAD%
7				(10^3)	
	303.15	8	0.10600	0.1576	23.222
	313.15	6	0.10871	0.1181	19.782
	323.15	7	0.10897	0.1300	13.684
8				(10^3)	
	303.15	7	0.12312	0.2915	29.282
	323.15	10	0.12525	0.2730	21.265
	343.15	10	0.10594	0.8422	22.884
9				(10^3)	
	308.00	5	0.13202	0.1410	8.124
	318.00	5	0.12644	1.5934	7.052
	328.00	5	0.11447	1.7051	7.830
10				(10^3)	
	308.00	5	0.10222	0.3792	9.120
	318.00	5	0.10513	0.1525	7.128
	328.00	5	0.10832	0.1032	2.631
11				(10^3)	
	308.00	5	0.10444	0.2104	5.846
	318.00	5	0.10036	0.2427	4.913
	338.00	5	0.10309	0.3737	9.197

Table B.2: Solid-fluid correlation using the SRK equation and the 2-parameter random mixing rules.

Solid	T[K]	N	k_{12}/A_{12}	AAD	AAD%
1				(10^3)	
	308.15	31	0.0688/-0.0796	0.5527	10.588
	318.15	20	0.0601/-0.0890	0.4993	11.642
	328.15	38	0.0492/-0.0999	1.1103	8.068
2				(10^4)	
	318.00	5	0.1500/0.0499	1.0020	8.280
	328.00	5	0.0149/0.0520	0.7193	8.640
	338.00	5	0.1487/0.0501	0.9504	11.210
	303.15	8	0.1530/0.0479	1.0212	9.508
	323.15	6	0.1492/0.0500	1.0405	8.853
	343.15	7	0.1497/0.0302	1.2884	36.600
3				(10^4)	
	303.15	4	0.2389/0.2010	0.0342	7.376
	323.15	10	0.2289/0.2010	0.0483	19.999
	343.15	9	0.1921/0.1599	0.0840	15.393
4				(10^3)	
	303.15	7	0.1592/0.1009	0.1396	10.011
	308.15	6	0.1589/0.1010	0.1372	12.283
	323.15	9	0.1609/0.1080	0.1202	15.106
	343.15	8	0.1607/0.1101	0.2595	19.494
5				(10^4)	
	308.15	7	0.2091/0.2011	0.1988	15.912
	323.15	7	0.1979/0.1912	0.1582	10.833
	343.15	8	0.1910/0.1900	0.1797	24.316
6				(10^2)	
	308.95	8	0.0402/-0.0802	0.0790	6.730
	318.55	8	0.0402/-0.0698	0.0768	2.935
	322.65	8	0.0479/-0.0488	0.0879	2.762

Table B.2 (cont'd)

Solid	T[K]	N	k_{12}/l_{12}	AAD	AAD%
7				(10^3)	
	303.15	8	0.1229/0.0332	0.0952	18.181
	313.15	6	0.1192/0.0199	0.0942	19.182
	323.15	7	0.1201/0.0198	0.1259	12.649
8				(10^3)	
	303.15	7	0.2099/0.1699	0.1246	19.163
	323.15	10	0.1922/0.1398	0.1375	22.651
	343.15	10	0.1844/0.1345	0.2168	11.393
9				(10^3)	
	308.00	5	0.1603/0.049	0.4666	2.437
	318.00	5	0.1480/0.0420	0.6761	2.921
	328.00	5	0.1478/0.0511	0.8561	6.144
10				(10^3)	
	308.00	5	0.1403/0.0775	0.1225	2.274
	318.00	5	0.1015/-0.0076	0.1467	6.723
	328.00	5	0.1081/-0.0004	0.1035	2.604
11				(10^3)	
	308.00	5	0.1599/0.1101	0.1822	7.516
	318.00	5	0.1519/0.0989	0.1685	8.743
	328.00	5	0.1491/0.0909	0.3317	13.072

Appendix C

CALIBRATION OF THE PRESSURE AND TEMPERATURE MEASUREMENTS

C.1 Calibration of the Pressure Transducers

The Dynisco pressure transducers (B1 : model 112743, max. 137.9 MPa or 20,000 psi and B2 : model 112851, max. 13.8 MPa or 2,000 psi) of Figure 3.1 were calibrated with a dead weight pressure tester (Testing Instrument Co. Inc.). The calibration curves for both transducers are shown in Figure C.1 and Figure C.2. In the figures, the reading-up curve is used when the pressure is increased whereas the reading-down curve is used when the pressure is decreased.

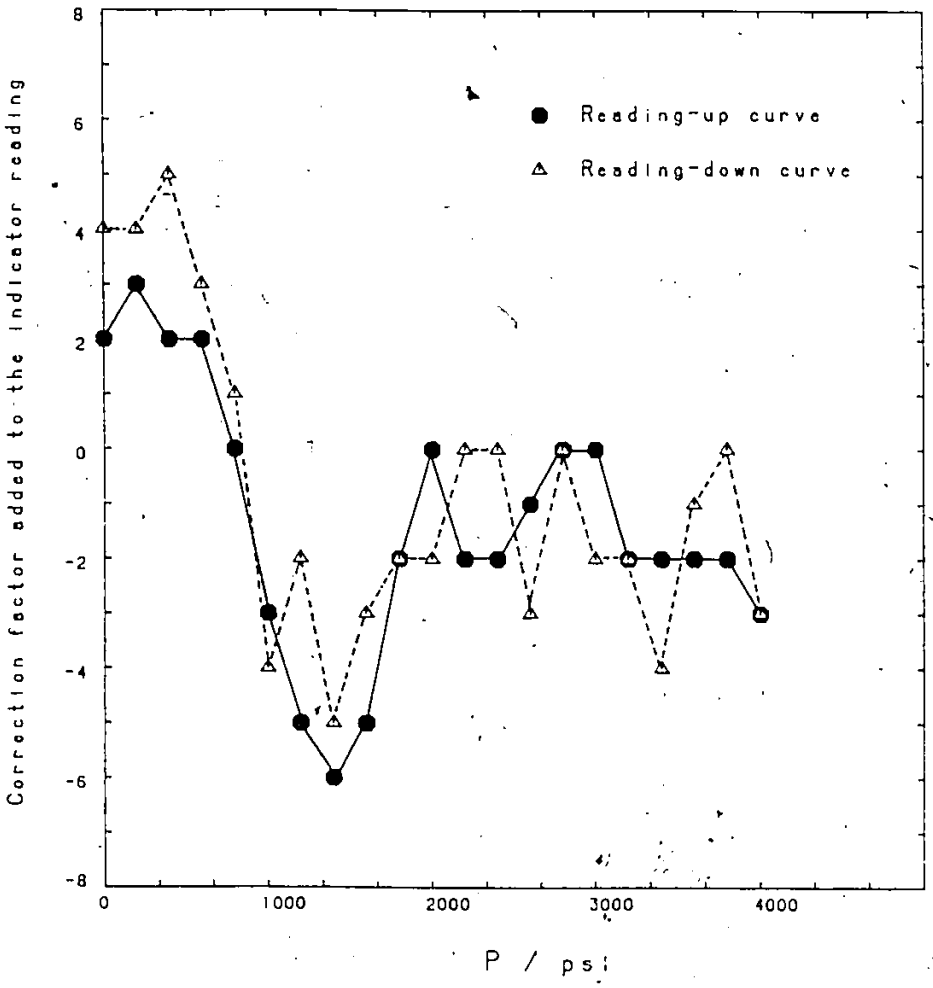

Figure C.1: Calibration curve for the B1 pressure transducer.

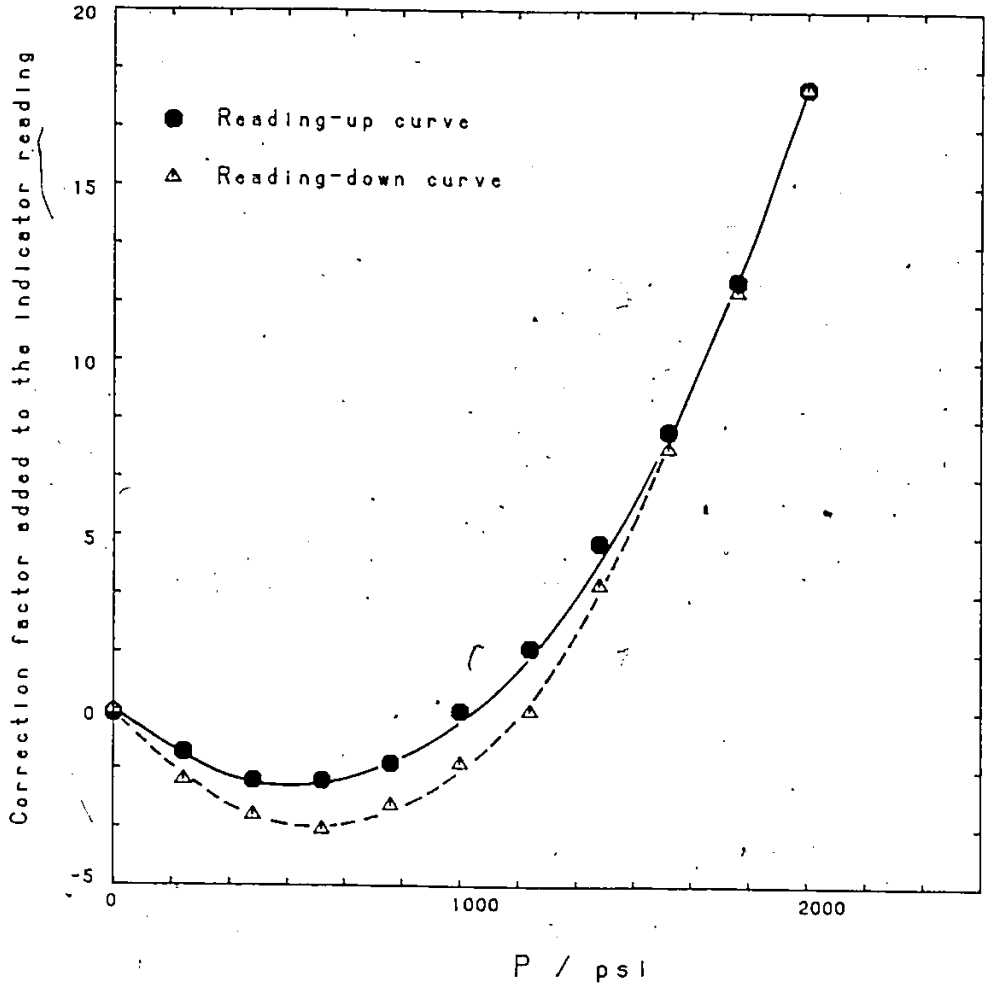

Figure C.2: Calibration curve for the B2 pressure transducer.

C.2 Calibration of the Hewlett-Parkard Quartz Thermometer

The quartz thermometer (model 2801A) with sensor of S.N. 1126-44 was calibrated at the triple point (0.010°C) of pure water with a platinum resistance thermometer (S.N. 1775701, calibrated 1968 IPTS scale, Leeds and Northrup). The resistance at the triple point of water (Ro) was found to be 25.58018 Ω at bridge temperature of 23.8°C. The platinum resistance thermometer was then used to calibrate the quartz thermometer with the following equation:

$$Rt/Ro = 1 + At + Bt^2 \qquad \text{(C-1)}$$

where $A = 3.98654 \times 10^{-3}$ and $B = -5.985 \times 10^{-7}$

In eq.(C-1), t is in °C and Rt is in Ω. The calibrated results at triple point as well as other temperatures are listed in Table C.1.

Table C.1: Calibration of the quartz thermometer.

Quartz thermometer reading [°C]	Estimated temp. using eq. (2-1) [°C]	Correction factor [°C]
-0.030	0.010 *	0.040
58.944	58.965	0.021
58.956	58.975	0.019
58.954	58.973	0.019

* Triple point of water.

Appendix D

CALIBRATION OF THE SAMPLER VOLUME FOR THE P-T-X MEASUREMENT

The calibration of the sampler volume in Figure 3.1 was performed in the following procedure. A known amount of carbon dioxide was expanded into the sample cylinder through valve 15 with valves 16, 11 and a closed (Figure 3.1). An increase in pressure of the high accuracy presure gauge was then recorded. Hence the calibration of the sampler volume could be obtained by expanding different amount of carbon dioxide into the sample cylinder. The calibrated results are shown in Table D.1 and Figure D.1.

Table D.1: Calibration of the sampler volume at 298.15 K.

n_2 [mole]	P at 298.15 K [KPa]	n_2/P [mole/KPa]
0.01100	60.31	1.824×10^{-4}
0.00870	47.49	1.832×10^{-4}
0.00721	39.50	1.825×10^{-4}
0.00581	31.57	1.840×10^{-4}
0.00320	17.30	1.850×10^{-4}
0.00113	5.86	1.928×10^{-4}

$\overline{(n_2/P)} = 1.850 \times 10^{-4}$ mole/KPa at 298.15 K.

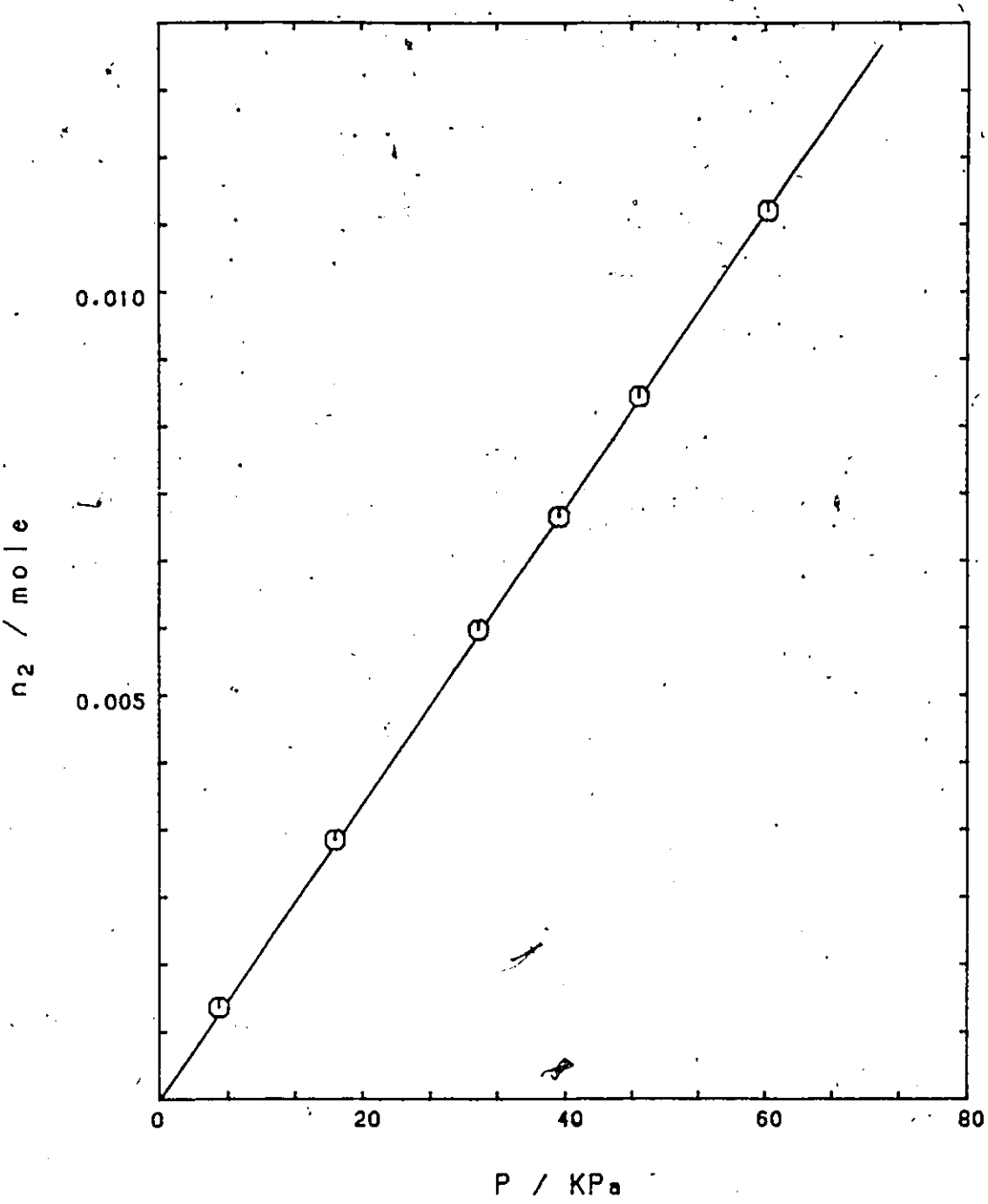

Figure D.1: Calibration curve of the sampler volume at 298.15 K.

Appendix E

RAW DATA AND SAMPLE CALCULATION

E.1 Raw Data of the Three-Phase Curve Measurement

The raw data of P-T measurement are listed in Table E.1 and the liquid-phase compositions (x_1) of the three-phase curve are listed in Table E.2. The sample calculation of the liquid-phase composition is illustrated in the following example.

For run no.8, when T = 334.46 K and P = 10.19 MPa, the increase in pressure was found to be 1.84 KPa at 298.15 K. From Appendix D, the number of moles of carbon dioxide was determined using the calibrated results,

$$n_2 = (1.84)(1.850 \times 10^{-4})$$
$$= 0.00034 \text{ moles}$$

Weight of naphthalene collected was found to be 0.06969 g. Thus the number of moles of naphthalene was determined as follows:

$$n_1 = 0.06969/128.18$$
$$= 0.00054 \text{ moles}$$

The liquid-phase composition was then easily determined from the above calculated results,

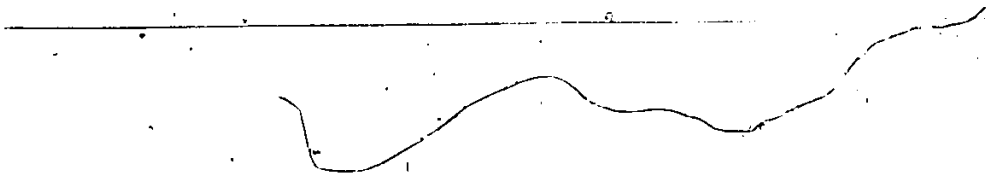

$$x_1 = n_1/(n_1+n_2)$$

$$= 0.6136$$

Table E.1: Raw data of the P-T measurement.

	First melting point		First freezing point			
	P [MPa]	T [K]	P [MPa]	T [K]	P [MPa]	T [K]
1	-	-	2.07	348.79	-	-
2	-	-	2.22	348.18	-	-
3	-	-	2.84	347.30	-	-
4	-	-	3.53	345.57	-	-
5	7.79	338.17	6.69	340.25	-	-
6	9.43	335.80	8.66	337.01	8.53	337.10
7	10.28	336.36	9.66	335.17	9.55	335.26
8	-	-	10.39	334.81	10.19	334.46
9	11.11	331.47	10.99	333.82	10.90	333.34
10	13.21	332.00	12.10	332.44	11.54	332.99
11	15.60	332.77	13.42	332.58	12.46	332.40
12	19.42	332.59	14.28	332.11	13.30	331.73
13	22.10	333.05	14.86	331.62	14.26	331.98
14	18.16	332.45	16.79	333.47	15.85	332.17
15	24.33	333.27	19.14	332.35	17.59	332.34
16	-	-	20.80	332.67	20.39	332.59
17	-	-	23.81	332.93	22.69	332.67
					21.92	332.83

Table E.2: Raw data of the liquid-phase composition.

No	P at 298.15 K [KPa]	n_2 [mole]	n_1 [mole]	x_1
8	1.84	0.00034	0.00054	0.6136
9	5.27	0.00097	0.00178	0.6473
12	12.00	0.00222	0.00163	0.4237
14	12.94	0.00239	0.00185	0.4296
15	15.62	0.00289	0.00140	0.3263
17	16.76	0.00310	0.00122	0.2824

E.2 Raw Data of the Solubility Measurement

Raw data of the solubility measurement at 308.15 K and 332.15 K are listed in Table E.3 and Table E.4 respectively. Sample calculation of the solubility data is illustrated in the following example using the solubility data at 308.15 K and 7.82 MPa.

experimental run time = 30 min.

volume of CO_2 collected = 3137.9 cm^3

ambient temperature = 295.93 K

The ambient pressure was assumed to be atmospheric pressure. Thus the number of moles of carbon dioxide was determined using ideal gas equation,

$$n_2 = (Pv)/(RT)$$
$$= \{(1)(3137.9)\}/\{(82.05)(295.93)\}$$
$$= 0.129231 \text{ moles}$$

Weight of naphthalene collected by the solid sampler was found to be 0.01941 g. The number of moles of naphthalene collected was therefore 0.000151 moles. Thus the vapour-phase mole fraction was determined as follows:

$$y_1 = n_1/(n_1+n_2)$$
$$= 0.001167$$

Table E.3: Solubility data at 308.15 K.

P [MPa]	Flowrate [cm^3/min]	n_2 [mole]	n_1 [mole]	y_1
7.82	105	0.129231	0.000151	0.001167
8.48	169	0.070076	0.000470	0.006657
	210	0.086717	0.000604	0.006913
	181	0.074437	0.000535	0.007137
9.93	136	0.055775	0.000556	0.009876
	183	0.074948	0.000760	0.010035
	98	0.039977	0.000398	0.009858
10.65	101	0.083867	0.000961	0.011331
	98	0.101558	0.001103	0.010739
	82	0.101416	0.001164	0.011349
11.27	192	0.079120	0.000949	0.011852
12.65	101	0.083160	0.001070	0.012706
14.09	103	0.085324	0.001280	0.014779
	139	0.144412	0.002002	0.013676
	109	0.067627	0.001001	0.014591
15.17	198	0.080811	0.001263	0.015386
	195	0.118972	0.001854	0.015345
16.30	109	0.112213	0.001802	0.015804
17.24	220	0.089948	0.001499	0.016392
20.78	114	0.117340	0.002080	0.017416
23.88	85	0.087592	0.001643	0.018409
28.36	118	0.097390	0.001881	0.018953
32.49	110	0.090275	0.001790	0.019439

Table E.4: Solubility data at 332.15 K.

P [MPa]	Flowrate [cm^3/min]	n_2 [mole]	n_1 [mole]	y_1
8.44	95	0.117445	0.000154	0.001307
10.20	113	0.139378	0.000351	0.002514
11.89	102	0.125613	0.000800	0.006326
12.50	103	0.105454	0.000884	0.008309
13.06	101	0.104056	0.001140	0.010833
	104	0.106852	0.001183	0.010948
15.13	114	0.117217	0.003082	0.025620
16.78	111	0.114543	0.004456	0.037444
20.44	85	0.116524	0.007803	0.062760
22.16	81	0.116069	0.008665	0.069467
26.02	77	0.116401	0.009362	0.074440
29.74	74	0.111863	0.009810	0.080628

Appendix F

THE COMPUTER PROGRAM

```
$JOB
C ------------------------------------------------------------
C
C     USING EXPERIMENTAL DATA TO FIND CONSTANTS OF
C           VAN LAAR EQUATION
C                 AND
C     CORRELATION OF T-X RELATION OF SOLID-LIQUID-GAS
C           COEXISTENCE CURVE
C
C ------------------------------------------------------------
      COMMON YA(50),ALPH(50),X1(50),DEV(50)
      COMMON SUM,SUM2,NOD
      DIMENSION DCO(4),CC(4)
      READ,NOD,DH,TM,R
      PRINT 12
   12 FORMAT('1',8X,'X1',8X,'GAMMA1'/)
      DO 1 J=1,NOD
         READ,X1(J),ALPH(J)
         PRINT 8,X1(J),ALPH(J)
    8    FORMAT('0',5X,F7.5,5X,F7.5)
    1 CONTINUE
C
      NO=2
          CC(1)=1.0
          CC(2)=1.0
          DCO(1)=1.0
          DCO(2)=1.0
      CALL DSO(CC,DCO,NO)
      PRINT 5
    5 FORMAT('0',20X,'**** PESULTS ****'/)
      PRINT 3,CC(1),CC(2),SUM2,SUM
    3 FORMAT('0',5X,'A12= ',F6.3,5X,'A21= ',F6.3/5X,'DEV X = ',F8.3,5X,'
     *SUM OF SUQARE = ',F10.8/)
      PRINT 15
   15 FORMAT('0',9X,'X1',8X,'GAMMA1',5X,'GAMMA1(CAL)',5X,'DEV X'/)
      DO 10 I=1,NOD
         PRINT 4,X1(I),ALPH(I),YA(I),DEV(I)
    4    FORMAT('0',5X,F8.3,5X,F8.3,5X,F8.3,5X,F8.3)
   10 CONTINUE
      PRINT 18
   18 FORMAT('1',10X,'****** T-X CORRELATION ******'/)
      A12=CC(1)
      A21=CC(2)
      X=0.05
      PRINT 50
   50 FORMAT('0',8X,'T(C) ',7X,'X1',9X,'GAMMA1',5X,'GAMMA2'/)
      WHILE( X .LE. 1.0 ) DO
         Y=A12/(1.+(A12*X)/(A21*(1.-X)))**2
         YB=A21/(1.+(A21*(1.-X))/(A12*X))**2
         YY=EXP(Y)
         YB=EXP(YB)
         YYX=ALOG(X*YY)
         DD=DH-R*TM*YYX
         T=TM*DH/DD-273.15
         PRINT 25,T,X,YY,YB
```

```
  25      FORMAT('0',5X,F6.2,5X,F7.5,5X,F7.4,5X,F7.4)
          X=X+3.05
        END WHILE
        STOP
        END
C
C
        SUBROUTINE DEV21(FOB,CO)
        COMMON YA(50),ALPH(50),X1(50),DEV(50)
        COMMON SUM,SUM2,NOD
        DIMENSION CO(4)
        A12=CO(1)
        A21=CO(2)
        SUM1=0.0
        SUM2=0.0
C
            DO 2 K=1,NOD
            Y=A12/(1.+(A12*X1(K))/(A21*(1.-X1(K))))**2
            YA(K)=EXP(Y)
            DEF=(ALPH(K)-YA(K))**2
            DEX=(ALPH(K)-YA(K))/ALPH(K)*100.0
            SUM1=SUM1+ABS(DEF)
            SUM2=SUM2+ABS(DEX)
            DEV(K)=DEX
   2        CONTINUE
            SUM2=SUM2/NOD
            SUM=SUM1/NOD
            FOB=SUM
            RETURN
            END
C
C
        SUBROUTINE DSO(CO,DCO,N)
         DIMENSION CO(4),DCO(4),CC(4),PJ(4),C2I(4),C2F(4)
            ICK = 0
             C2I(1) =  0.5
             C2F(1) = 5.00
             C2I(2) =  0.5
             C2F(2) = 5.00
         DO 200 I = 1,N
        CC(I)=CO(I)
        PJ(I)=1.
 200    CONTINUE
   3    CALL DEV21(FO,CO)
        GO TO 15
  15    CONTINUE
        WRITE(6,900) (CO(I),I=1,N),FO
 900    FORMAT(1H0,'INITIAL',8E12.4)
        DO 40 K=1,5
            DO 220 I = 1,N
        DCO(I)=DCO(I)/10.
 220        CONTINUE
  20        J = 0
             DO 50 I = 1, N
             MHQ = 0
```

```
   60       CO(I) = CC(I)+ DCO(I)*PJ(I)
             IF (CO(I) .LE. C2I(I)) CO(I) = C2I(I)
             IF (CO(I) .GE. C2F(I)) CO(I) = C2F(I)
           CALL DEV21(F,CO)
   35 CONTINUE
      MHQ=MHQ+1
      IF( F.LT.F0 ) GO TO 70
      PJ(I)=-PJ(I)
      IF( MHQ-1 ) 60,60,80
   80 CO(I)=CC(I)
                    J = J + 1
      GO TO 50
   70 CC(I)=CO(I)
      F0=F
   50 CONTINUE
         IF ( J .NE. N) GO TO 20
      WRITE(6,1000) (CO(I),I=1,N),F0
 1000 FORMAT(1H ,'E.OF S.',8E12.4)
   40 CONTINUE
         ICK = 1
  103 CALL DEV21(F0,CO)
      GO TO 120
  120 CONTINUE
      WRITE(6,1100) (CO(I),I=1,N),F0
 1100 FORMAT(1H ,'RESULTS',8E12.4)
      RETURN
      END
$ENTRY
```

```
C
C
C ------------------------------------------------------------------
C
C       USING SOAVE-REDLICH-KWONG EQUATION OF STATES AND
C
C       1-PARAMETER AND 2-PARAMETER RANDOM MIXING RULES
C
C       TO CORRELATE SOLID-FLUID EQUILIBRIUM
C
C ------------------------------------------------------------------
C -                                                                -
C -       MIXING RULES :                                         -
C -       --------------                                         -
C -                                                                -
C -       JMIX   =  1   1-P RANDOM MIXING                        -
C -                                                                -
C -                 2   2-P RANDOM MIXING                        -
C -                                                                -
C ------------------------------------------------------------------
C
C
C ---------------------------------------------------
C -                                                 -
C -          MAIN PROGRAM                           -
C -                                                 -
C ---------------------------------------------------
C
      IMPLICIT REAL*8(A-H,O-Z)
      DIMENSION TITLE(20),COO(4),DCO(4)
      COMMON /BK1/ T,P(50),X1(50),Y1(50),YCL(50),YDO(50),YDY(50),
     *             AVY,R,NOD,JMIX
      COMMON /BK2/ SA1,SA2,SB1,SB2
      COMMON /BK3/ TC1,TC2,CIJ,BIJ,PS,VS
      COMMON /BK4/ AVPA,AVYA,RMSY
C
C --------  MIXING RULES  ------------------------
C
      JMIX = 1
C
C ---------------------------------------------------
C
    1 READ(5,150,END=999) (TITLE(I),I=1,18)
  150 FORMAT(18A4)
      WRITE(6,900) (TITLE(I),I=1,18)
  900 FORMAT(1H1,18A4)
      READ(5,101) NCOMP,NONTUM,IJK,R
  101 FORMAT(3I5,F10.0)
      IF( NCOMP.LE.0 ) GO TO 1
      WRITE(6,901)
  901 FORMAT(1H0,'INPUT DATA:'//)
      READ(5,102) PC1,VC1,TC1,W1,NA11,NA12,NA13,NA14
      READ(5,102) PC2,VC2,TC2,W2,NA21,NA22,NA23,NA24
  102 FORMAT(4F8.0,17X,4A4)
      WRITE(6,789)
```

```
  789 FORMAT(1H0,7X,'PC',9X,'VC',9X,'TC',12X,'W'/)
      WRITE(6,902) PC1,VC1,TC1,W1,NA11,NA12,NA13,NA14
      WRITE(6,902) PC2,VC2,TC2,W2,NA21,NA22,NA23,NA24
      WRITE(6,111) JMIX
  111 FORMAT(9X,'JMIX =',I4/)
  902 FORMAT(1H ,4F12.6,10X,4A4)
      READ(5,100) A,B,C
      READ(5,106) VS
      READ(5,103) T,PSI,IT
      READ(5,104) IJK
  103 FORMAT(2F10.0,5I2)
  104 FORMAT(10X,I2)
      IF( IT.EQ.1 ) T=(T-32.)/1.8+273.15
      IF( IT.EQ.2 ) T=T+273.15
      PSS = A-B/(T+C)
      PS = 10**PSS/1.01325
C     PS = DEXP(A-B/(T-273.15+C))/760.0
      WRITE(6,903) T
  903 FORMAT(1H0,5X,'T=',F10.4,' K')
      WRITE(6,555) A,B,C
  555 FORMAT(1H0,5X,'ANTIONE COEFF. = ',3E15.5/)
      WRITE(6,666) PS
  666 FORMAT(1H0,5X,'SOLID VAPOUR PRESSURE = ',E12.5,2X,'ATM'/)
      WRITE(6,699) VS
  699 FORMAT(1H0,5X,'MOLAR VOLUME = ',E12.5,2X,'CC'/)
      WRITE(6,667)
  667 FORMAT(1H0,12X,'P(ATM)',12X,'Y1(EXP)'/)
      NOD=1
   32 READ(5,100) P(NOD),X1(NOD),Y1(NOD)
  100 FORMAT(7F10.0)
      IF( P(NOD) ) 33,34,34
   34 IF( NQNTUM.EQ.1 ) X1(NOD)=Y1(NOD)/X1(NOD)
      IF( NQNTUM.EQ.3 ) X1(NOD) = 1.-X1(NOD)
      IF( NQNTUM.EQ.3 ) Y1(NOD) = 1.-Y1(NOD)
      IF( NQNTUM.EQ.2 ) GO TO 811
  812 CONTINUE
      IF( IJK.EQ.0 ) P(NOD)=P(NOD)/14.697
      IF( IJK.EQ.2 ) P(NOD)=P(NOD)*1000./6.895/14.697
      IF( IJK.EQ.3 ) P(NOD)=P(NOD)/760.
      IF( IJK.EQ.5 ) P(NOD)=P(NOD)/1.01325
      WRITE(6,904) NOD,P(NOD),Y1(NOD)
  904 FORMAT(1H ,I3,5X,F10.2,5X,F15.6)
      NOD=NOD+1
      GO TO 32
  811 CONTINUE
      TEMP=(1.-Y1(NOD))/(X1(NOD)-Y1(NOD))
      Y1(NOD)=TEMP*X1(NOD)
      X1(NOD)=TEMP
      GO TO 812
   33 NOD=NOD-1
C
C
C ----   INPUT PURE COMPONENT PARAMETERS  ---------
C
C
```

```
      SB1=0.08664*R*TC1/PC1
      SB2=0.08664*R*TC2/PC2
C     ALPH1=0.47978+1.57624*W1-0.19394*W1**2+0.02779*W1**3
C    1       -0.0016577*W1**4-0.00013153*W1**5
C     ALPH2=0.47978+1.57624*W2-0.19394*W2**2+0.02779*W2**3
C    1       -0.0016577*W2**4-0.00013153*W2**5
      ALPH1=0.48+1.574*W1-0.176*W1**2
      ALPH2=0.48+1.574*W2-0.176*W2**2
      SA1=0.42747*(R*TC1)**2/PC1*(1.+ALPH1*(1.-DSQRT(T/TC1)))**2
      SA2=0.42747*(R*TC2)**2/PC2*(1.+ALPH2*(1.-DSQRT(T/TC2)))**2
C
C ------   SPECIFY NO. OF PARAMETER AND   ----------
C ------              STARTING VALUES     ----------
C
      N = JMIX
      COO(1) =  0.100000
      COO(2) =  0.0000000
      DCO(1) = 0.1
      DCO(2) = 0.1
C
      CALL DSO(COO,DCO,N)
C     CALL DEV21(FCB,COO)
C
      WRITE(6,1055) CIJ,BIJ
      WRITE(6,1000) T,AVY
      WRITE(6,1050) AVYA
      WRITE(6,1057) RMSY
      WRITE(6,688)
      DO 20 I=1,NOD
   20 WRITE(6,1100) P(I),Y1(I),YCL(I),YDD(I),YDY(I)
      GO TO 1
  999 STOP
  688 FORMAT(//12X,'P(ATM)',12X,'Y1(EXP)',10X,'Y1(CAL)',12X,'DEV',11X,'X
     * DEV')
 1000 FORMAT(//2X,'TEMP=',E13.5,5X,
     1'  AVXDEV=',4E13.5//)
 1055 FORMAT(//2X,' K12=',E13.5,2X,'L12 =',E13.5//)
 1050 FORMAT(//2X,23X,'  AV.ARS=',2E13.5//)
 1057 FORMAT(//2X,23X,'  RMS   =',2E13.5//)
 1100 FORMAT(1H ,6E18.5)
      END
C
C
C ---------------------------------------------
C -                                           -
C -         SORTING X(1), X(2) AND X(3)       -
C -                                           -
C ---------------------------------------------
C
C
      SUBROUTINE TRTON(A,X,N)
      IMPLICIT REAL*8(A-H,O-Z)
      DIMENSION A(3),X(3)
      CALL TRNLQ(A,X,N)
```

```
      IF( N .NE. 1 ) GO TO 10
      X(2)=X(1)
      X(3)=X(1)
      RETURN
   10 XM=X(1)
      IF( X(2) .GT. X(1) ) GO TO 11
      X(1)=X(2)
      X(2)=XM
   11 XM=X(1)
      IF( X(3) .GT. X(1) ) GO TO 12
      X(1)=X(3)
      X(3)=XM
   12 XM=X(3)
      IF( X(3) .GT. X(2) ) GO TO 13
      X(3)=X(2)
      X(2)=XM
   13 RETURN
      END
C
CC
C ---------------------------------------------------
C -                                                 -
C -                SOLVE ROOTS OF                   -
C -         Z**3-Z**2+(A-B-B**2)*Z-AB = 0           -
C -                                                 -
C ---------------------------------------------------
C
C
      SUBROUTINE TRNLO(A,X,N)
      IMPLICIT REAL*8(A-H,O-Z)
      DIMENSION A(3),X(3)
      PAI=3.14159265358900
      E=(3.*A(2)-A(1)*A(1))/9.
      F=(2.*A(1)**3-9.*A(1)*A(2)+27.*A(3))/27.
      D=F*F+4.*E*E*E
      IF( D ) 1,2,2
    2 F1=(-F+DSQRT(D))/2.
      F2=(-F-DSQRT(D))/2.
      X(1)=-A(1)/3.
      IF( F1 .NE. 0. ) X(1)=X(1)+F1/DABS(F1)**(2./3.)
      IF( F2 .NE. 0. ) X(1)=X(1)+F2/DABS(F2)**(2./3.)
      N=1
      GO TO 10
    1 R=DSQRT(-E*E*E)
      COR=-F/2./R
      THETA=DARCOS(COR)
      XX=2.*R**(1./3.)
      XY=-A(1)/3.
      X(1)=XX*DCOS(THETA/3.)+XY
      X(2)=XX*DCOS((THETA+2.*PAI)/3.)+XY
      X(3)=XX*DCOS((THETA+4.*PAI)/3.)+XY
      N=3
   10 RETURN
      END
C
```

```
C
C ------------------------------------------------
C -                                              -
C -         DEVIATION FUNCTION                   -
C -                                              -
C ------------------------------------------------
C
C
      SUBROUTINE DEV21(FOR,COO)
      IMPLICIT REAL*8(A-H,O-Z)
      COMMON /BK1/ T,P(50),X1(50),Y1(50),YCL(50),YDD(50),YDY(50),
     *             AVY,R,NOD,JMIX
      COMMON /BK2/ SA1,SA2,SB1,SB2
      COMMON /BK3/ TC1,TC2,CIJ,BIJ,PS,VS
      COMMON /BK4/ AVPA,AVYA,RMSY
      DIMENSION AX(3),X(3),COO(4)
      AVYA=0.
      RMSY=0.0
      NUM=0
      FOR=0.0
      YS=0.0
      GO TO ( 126,129 ),JMIX
C
C --------  1-P RANDOM MIXING  -------------------
C
  126 CIJ=COO(1)
      SA12=(1.-CIJ)*DSQRT(SA1*SA2)
      GO TO 113
C
C --------  2-P RANDOM MIXING  -------------------
C
  129 CIJ=COO(1)
      BIJ=COO(2)
      SA12=(1.-CIJ)*DSQRT(SA1*SA2)
      SB12=(1.-BIJ)*(SB1+SB2)/2.
      GO TO 113
C
  113 DO 10 I=1,NOD
      POLD=P(I)
      YC1=Y1(I)
      YC2=1.-YC1
      IT=0
      DYF=0.0
C
C ---------  ITERATION OF Y1 --------------------
C
   13 CONTINUE
      IT=IT+1
      GO TO ( 101,102 ),JMIX
C
C ------  1-P RANDOM MIXING  --------------------
C
  101 SA=YC1**2*SA1+YC2**2*SA2+2.*YC1*YC2*SA12
      SB=YC1*SB1+YC2*SB2
      GO TO 125
```

```
C
C ------   2-P RANDOM MIXING  ---------------------
C
  102 SA=YC1**2*SA1+YC2**2*SA2+2.*YC1*YC2*SA12
      SB=YC1**2*SB1+YC2**2*SB2+2.*YC1*YC2*SB12
      GO TO 125
C
  125 A=SA*POLD/(R*T)**2
      B=SB*POLD/(R*T)
      AX(1)=-1.
      AX(2)=A-B-B**2
      AX(3)=-A*B
      CALL TRTON(AX,X,NN)
      ZV=X(3)
C     IF ( ZV .LE. B ) ZV=X(2)
C     IF ( ZV .LE. B .OR. POLD .LT. PC2 ) ZV=X(3)
C
      GO TO ( 123,124 ),JMIX
C
C --------  CALCULATE FUGACITY COEFFICIENT  ------
C
  123 FV1=SB1/SB*(ZV-1.)-DLOG(ZV-B)-A/B*(2.*(YC1*SA1+YC2*SA12)/SA
     1     -SB1/SB)*DLOG(1.+B/ZV)
      FV2=SB2/SB*(ZV-1.)-DLOG(ZV-B)-A/B*(2.*(YC2*SA2+YC1*SA12)/SA
     1     -SB2/SB)*DLOG(1.+B/ZV)
      GO TO 155
C
  124 VV=ZV*R*T/POLD
      A1=2.*(YC1*SA1+YC2*SA12)
      B1=2.*(YC1*SB1+YC2*SB12)
      A2=2.*(YC2*SA2+YC1*SA12)
      B2=2.*(YC2*SB2+YC1*SB12)
      FV1=(B1-SB)/(VV-SB)+SA/(P*T*(VV+SB))*(1.-B1/SB)-DLOG(ZV-B)
     1              -A/B*(1.+A1/SA-B1/SB)*DLOG(1.+B/ZV)
      FV2=(B2-SB)/(VV-SB)+SA/(P*T*(VV+SB))*(1.-B2/SB)-DLOG(ZV-B)
     1              -A/B*(1.+A2/SA-B2/SB)*DLOG(1.+B/ZV)
      GO TO 155
C
  155 FV1=DEXP(FV1)
      FV2=DEXP(FV2)
C
C --- EVALUATE SOLID COMPOSITION IN SUPERCRITICAL GAS ---
C
      YN1=PS/POLD/FV1*DEXP(VS/R/T*(POLD-PS))
      DYF=(YC1-YN1)/YC1
C
C ---   COMPARE Y1(ASSUMED) AND Y1(CALCULATED)  ---
C
      IF ( DABS(DYF) .LE. 1.0E-03 ) GO TO 30
C
      IF ( IT .GT. 200 ) GO TO 999
      IF ( YN1 .LE. 0.0 ) YN1=1.E-05
      IF ( YN1 .GE. 0.2 ) YN1=0.02
      YC1=(YN1+YC1)/2.
      YC2=1.-YC1
```

```
      GO TO 13
C
C -----  EVALUATE DEVIATION FUNCTION  ------------
C
   30 CONTINUE
      YC1=YN1
      YCL(I)=YC1
      DYY=(Y1(I)-YC1)/Y1(I)
      YDY(I)=(Y1(I)-YCL(I))/Y1(I)*100.
      YDD(I)=Y1(I)-YCL(I)
      NUM=NUM+1
      YS=YS+DABS(YDY(I))
      AVYA=AVYA+DABS(Y1(I)-YCL(I))
      RMSY = RMSY + (YDY(I)*Y1(I)/100.)**2
      GO TO 10
  999 WRITE(6,1000)      CIJ,RIJ,POLD,YC1,YN1
 1000 FORMAT(1H ,'*** CONVERGENCE PROBLEM ***',5E13.5/)
C
   10 CONTINUE
C
      IF( NUM.EQ.0 ) GO TO 11
      AVY=YS/NUM
      AVYA=AVYA/NUM
      RMSY = (RMSY/NUM)**0.5
C
C -------  OBJECTIVE FUNCTION  ------------------
C
      FOB=AVYA
C
   11 IF( NUM.EQ.0 ) FOB=1.E20
      IF( NUM.NE.NOD ) FOB=FOB+100.00
      RETURN
      END
C
C
C ---------------------------------------------------
C -                                                 -
C -          OPTIMIZATION SUBROUTINE                -
C -                                                 -
C ---------------------------------------------------
C
C
      SUBROUTINE DSO(CO,DCO,N)
      IMPLICIT REAL*8(A-H,O-Z)
      DIMENSION CO(4),DCO(4),CC(4),PJ(4),C2I(4),C2F(4)
           ICK = 0
           C2I(1) = -0.1
           C2F(1) = 0.35
           C2I(2) = -0.3
           C2F(2) = 0.3
       DO 200 I = 1,N
      CC(I)=CO(I)
      PJ(I)=1.
  200  CONTINUE
C
```

```
    3 CALL DEV21(F0,CO)
      GO TO 15
C
   15 CONTINUE
      WRITE(6,900) (CC(I),I=1,N),F0
  900 FORMAT(1H0,'INITIAL',8F12.4)
C
      DO 40 K=1,5
         DO 220 I = 1,N
      DCO(I)=DCO(I)/10.
  220    CONTINUE
C
   20    J = 0
         DO 30 I = 1, N
         MHQ = 0
   60    CO(I) = CC(I)+ DCO(I)*PJ(I)
           IF (CO(I) .LE. C2I(I)) CO(I) = C2I(I)
           IF (CO(I) .GE. C2F(I)) CO(I) = C2F(I)
         CALL DEV21(F,CO)
   35 CONTINUE
      MHQ=MHQ+1
      IF( F.LT.F0 ) GO TO 70
      PJ(I)=-PJ(I)
      IF( MHQ-1 ) 60,60,80
   80 CO(I)=CC(I)
                    J = J + 1
      GO TO 50
C
   70 CC(I)=CO(I)
      F0=F
C
   50 CONTINUE
C
           IF ( J .NE. N) GO TO 20
      WRITE(6,1000) (CO(I),I=1,N),F0
 1000 FORMAT(1H ,'E.OF S.',8E12.4)
   40 CONTINUE
C
         ICK = 1
  103 CALL DEV21(F0,CO)
      GO TO 120
  120 CONTINUE
      WRITE(6,1100) (CO(I),I=1,N),F0
 1100 FORMAT(1H ,'RESULTS',8F12.4)
      RETURN
      END
```

Appendix G

EQUIPMENT SUPPLIERS

(1) Automatic boost pump.

Manufacturer :	Futurecraft Corp., California
Supplier :	Hydrocon Co. 10690 Shadow Wood. No. 122 Houston, Tx 77043 Tel: (713)932-8240
Model :	90739
Working pressure :	68.9 MPa

(2) High pressure view cell.

Manufacturer :	Jerguson Gauge and Valve Co.
Supplier :	Peacock Inc. C.P. 1040, Station "A" Montreal, Quebec H3C 2X5
Model :	11T51

Working pressure : 68.9 MPa

(3) Pressure transducer.

Manufacturer : Dynisco

Model : 112851, 112743

Working pressure : 13.8 MPa, 137.9 MPa

(4) Precision temperature controller.

Manufacturer : Bayley Instrument Co., California

Model : 250

Temperature range : -200 to 100°C

(5) Quartz thermometer.

Manufacturer : Hewlett Packard

Model : 2801A

Temperature range : -80 to 250°C